Development 126, 1753-1768 (1999)
Printed in Great Britain © The Company of Biologists Limited 1999
DEV4139

Early embryonic lethality in *Bmp5;Bmp7* double mutant mice suggests functional redundancy within the 60A subgroup

Mark J. Solloway and Elizabeth J. Robertson*

Department of Molecular and Cellular Biology, Harvard University, Cambridge, MA 02138, USA
*Author for correspondence (e-mail: ejrobert@husc.harvard.edu)

Accepted 1 February; published on WWW 17 March 1999

SUMMARY

Members of the BMP family of signaling molecules display a high conservation of structure and function, and multiple BMPs are often coexpressed in a variety of tissues during development. Moreover, distinct BMP ligands are capable of activating common pathways. Here we describe the coexpression of two members of the 60A subfamily of BMPs, *Bmp5* and *Bmp7*, at a number of different sites in the embryo from gastrulation onwards. Previous studies demonstrate that loss of either *Bmp5* or *Bmp7* has negligible effects on development, suggesting these molecules functionally compensate for each other at early stages of embryonic development. Here we show this is indeed the case. Thus we find that *Bmp5;Bmp7* double mutants die at 10.5 dpc and display striking defects primarily affecting the tissues where these factors are coexpressed. The present analysis also uncovers novel roles for BMP signaling during the development of the allantois, heart, branchial arches, somites and forebrain. *Bmp5* and *Bmp7* do not appear to be involved in establishing pattern in these tissues, but are instead necessary for the proliferation and maintenance of specific cell populations. These findings are discussed with respect to potential mechanisms underlying cooperative signaling by multiple members of the TGF-β superfamily.

Key words: BMP, TGF-β, Cell signalling, Early embryonic development, Mouse

INTRODUCTION

The secreted signaling molecules of the transforming growth factor-beta (TGF-β) superfamily play critical roles in the specification and patterning of cells during embryogenesis. Composed of greater than 30 members, the superfamily has been divided into several subgroups according to the extent of homology in the mature ligand domains. The largest subgroup constitutes the bone morphogenetic proteins (BMPs). Initially implicated as regulators of bone formation, subsequent analysis has revealed that BMP family members are important mediators of inductive tissue interactions throughout embryogenesis. Individual BMPs can contribute distinct activities at multiple timepoints and in different cellular contexts during the development of an organism. For example, Bmp4 instructively promotes neurogenesis in neural crest stem cells (Shah et al., 1996), inhibits epithelial cell proliferation in the embryonic mouse lung (Bellusci et al, 1996), and induces interdigital apoptosis in the developing limb bud (Gañan et al., 1996). Additionally, multiple BMPs are often coexpressed in tissues displaying increased cell proliferation, differentiation, or apoptosis (Liem et al., 1995; Lyons et al., 1995; Dudley and Robertson, 1997; Furuta et al., 1997). BMP family members have been implicated in the development of almost all vertebrate organs and tissues, as well as in early embryonic axis determination (for review see Hogan, 1996).

Recent data demonstrate complex in vivo functions mediated by individual BMP family members. In particular, closely related BMP ligands have been shown to elicit distinct cellular responses. For example, implanting beads coated with Bmp2, 4, or 7 causes the induction of *Msx1* expression in anterior neural plate explant cultures, but Bmp6-coated beads have no effect (Furuta et al., 1997; Shimamura and Rubenstein, 1997). Similarly, exposure of sympathoadrenal cells to media containing Bmp2 or Bmp4 results in dose-dependent apoptosis whereas Bmp7 has no effect on cell survival (Song et al., 1998). Thus, specific embryonic cell types can distinguish between mature ligands sharing over 90% identity (Bmp6 and Bmp7) whereas other subpopulations are capable of responding identically to ligands which are only 60% identical (comparing Bmp2 or Bmp4 to Bmp7). However, relatively little is known about the molecular mechanisms by which multiple BMP signals are interpreted and integrated by any given cell.

Distinct TGF-β ligands have been shown to activate common downstream pathways (for review see Massagué, 1998). TGF-β signaling is mediated by a family of serine/threonine receptor kinases that fall into two classes: type I and type II. Ligand binding leads to the association of these two receptor types, phosphorylation of the type I receptor by the type II receptor, and subsequent propagation of the intracellular signal. Seven type I or activin-like kinases (ALKs) and five type II receptors have been identified in

vertebrates, yet only ALK-2, ALK-3, and ALK-6 appear to specifically transduce BMP signals. Thus, responses may be determined by both the stoichiometry of ALKs in the cell and their ability to form complexes with particular type II receptors. Transfected cells expressing ALK-3 can bind Bmp2, Bmp4 and Bmp7 with variable affinities (ten Dijke et al., 1994), and a loss-of-function mutation in ALK-3 leads to a profound disruption of early embryonic development and the complete absence of mesoderm formation (Mishina et al., 1995). This phenotype is more severe than those caused by mutations in either *Bmp2*, *Bmp4* or *Bmp7* (Dudley et al., 1995; Luo et al., 1995; Winnier et al., 1995; Zhang and Bradley, 1996), suggesting that closely related family members may be able to partially compensate for one-another by signaling through the same receptor complex. Studies of the 'pathway' Smads, transcriptional activators essential for TGF-β-related signal transduction, strengthen the idea that different BMP ligands channel into the same downstream pathway. Like the Alks, the pathway Smads fall into two distinct categories: Smad1 and presumably its two close homologues Smad5 and Smad8 are BMP receptor substrates, whereas Smad2 and Smad3 are substrates of the related TGF-β and activin receptors in vertebrates (Kretzschmar and Massagué, 1998). In sum, the effects seen with the various BMP family members are highly dependent on the tissue/cell type being investigated, and likely reflect the available repertoire and expression levels of receptors, Smads and downstream effector molecules.

Bmp2 and Bmp4 are expressed early in postimplantation mouse embryos (Winnier et al., 1995; Lyons et al., 1995; Waldrip et al., 1998), and targeted mutations in these two genes cause defects that correlate well with their respective expression domains (Winnier et al., 1995; Zhang and Bradley, 1996). In contrast, mutations in members of the *60A* subfamily consistently display less severe phenotypes than would be predicted from their broad expression patterns. Loss-of-function mutations in *Bmp5* map to the classic mouse *short ear* (*se*) locus (Kingsley et al., 1992). *se* mice are viable as homozygotes and display defects in the development of specific bone elements and several soft tissues (Green and Green, 1942; Green, 1951; King et al., 1994). Interestingly, *Bmp5* transcripts are expressed at the earliest stages of skeletal development in most bones, but only a subset of these are affected. Similarly, although *Bmp6* transcripts are present at many diverse tissue sites (Dudley and Robertson, 1997; Furuta et al., 1997), *Bmp6* mutants are homozygous viable and exhibit a slight delay in the growth of the sternum (Solloway et al., 1998). *Bmp7* is also expressed at numerous sites throughout development (Lyons et al., 1995). However, loss of *Bmp7* function causes focal defects in the eye, kidney and skeleton (Dudley et al., 1995; Luo et al., 1995) at sites where *Bmp7* appears to be the only BMP present (Dudley and Robertson, 1997). These relatively subtle developmental defects provide evidence that related BMP ligands functionally compensate for the absence of a BMP normally expressed in the same tissue.

Here we have used a genetic approach to test for functional redundancy of BMP family members in the developing mouse embryo. The present study demonstrates that *Bmp5* and *Bmp7* are strikingly coexpressed from the initiation of gastrulation to 10.5 dpc. Both transcripts are present in the heart, allantois, rostral neurectoderm and subjacent mesenchyme, lateral plate mesoderm and branchial arches. Analysis of *Bmp5*; *Bmp7* double mutants reveals deficits in chorio-allantoic fusion and heart development leading to embryonic lethality by 9.5 to 10.5 days postcoitum (dpc). In addition, our studies have uncovered novel requirements for *Bmp5* and *Bmp7* signaling in the growth of the branchial arches, closure of the rostral neural tube, generation or maintenance of neural crest and patterning of the somites. This potent genetic interaction between two closely related BMPs provides strong evidence that these molecules share largely overlapping activities at diverse tissue sites during mouse embryogenesis.

MATERIALS AND METHODS

Mouse strains

The se^{GnJ} mutation is a null allele at the *Bmp5* locus (Kingsley et al., 1992). These mice were obtained from the Jackson Laboratory, Bar Harbor, Maine, and a homozygous breeding colony was established on an outbred background. The null *Bmp7* allele ($Bmp7^{m1Rob}$) used in this study has been described previously (Dudley et al., 1995) and was also maintained on an outbred background. Double mutants were initially generated by crossing se^{GnJ} homozygotes to $Bmp7^{m1Rob}$ heterozygotes and intercrossing the se^{GnJ}*/+; Bmp7*/+ F_1 progeny. We observed that *se/se; Bmp7*/+ animals were healthy, fertile and phenotypically identical to *se* homozygotes. In order to increase the yield of double mutants, all further analysis was done by intercrossing *se/se; Bmp7*/+ mice to generate *se/se; Bmp7/Bmp7*, *se/se; Bmp7*/+ and *se/se;* +/+ progeny in the ratio 1:2:1. During the course of this study, no differences were ever noted between *se/se; Bmp7*/+, *se/se;* +/+ and wild-type embryos prior to 12.5 dpc, so these groups were pooled for use as controls.

DNA sample collection and genotyping procedures

Yolk sac samples were collected during dissection, washed, and digested overnight at room temperature in 50 μl of lysis buffer (50 mM KCl, 10 mM Tris-HCl at pH 8.3, 2.5 mM $MgCl_2$, 0.1 mg/ml gelatin, 0.45% NP-40, 0.45% Tween-20, 1.4 mg/ml Proteinase K). Subsequently, samples were boiled for 10 minutes, and 1 μl of digested material was used per PCR reaction as described below.

The classical se^{GnJ} mutation contains a nonsense mutation in *Bmp5* (King et al., 1994) which introduces an *αTaqI* restriction site polymorphism. A PCR-based genotyping assay that detects this polymorphism was used as previously described by Solloway et al. (1998). Genotyping for the targeted $Bmp7^{m1Rob}$ allele was also carried out as described previously (Dudley et al., 1995).

Histology, in situ hybridization and TUNEL analysis

Embryos were fixed in 4% paraformaldehyde in PBS at 4°C overnight, followed by dehydration through a graded methanol series. The material was cleared in xylene and embedded in Fibrowax (BDH Laboratory Supplies, England). Samples were sectioned at 7-10 μm, and sections collected on Tespa-treated glass slides. Sections for histology were stained with hematoxylin and eosin using standard procedures.

Whole-mount TUNEL was carried out as described by Conlon et al. (1995). Whole-mount in situ hybridization using digoxigenin-labelled RNA was performed as described by Wilkinson (1992). Comparisons were made of embryos with similar numbers of somites. Antisense probes specific for *Bmp5* (Solloway et al., 1998), *Bmp7* (Solloway et al., 1998), *Wnt-1* (Parr et al., 1993), *Pax-3* (Goulding et al., 1991), *Shh* (Echelard et al., 1993), *MLC2A* (Kubalak et al., 1994), *Fgf-8* (Heikinheimo et al., 1994), *M-twist* (Füchtbauer, 1995) and *AP-2* (Zhang et al., 1996a) were used as described. The *Wnt8b* probe was

kindly provided by Scott Lee and Andrew McMahon (S. Lee and A McMahon, personal communication). After initial photography, embryos were dehydrated, embedded and sectioned as described above. Sections were photographed using a Leitz DMR photomicroscope and Ektachrome 160T color slide film.

Neural crest outgrowth assay

Neural tube isolation and culture was performed essentially as described by Stemple and Anderson (1992). Trunk sections were isolated from 9.0 dpc embryos derived from timed matings between se^{GnJ}/se^{GnJ}; *Bmp7*/+ mice. After digestion with 100 U/ml collagenase (Worthington Biochemical) on ice, neural tubes were carefully triturated through a glass pipette until they were completely clean of contaminating cells. Neural tubes were plated onto tissue culture dishes coated with human plasma fibronectin (GibcoBRL, MD) and cultured in a humidified 5% CO_2 incubator for 5 days in Dulbecco's modified Eagle's medium (DMEM) supplemented with 10% fetal calf serum, penicillin (10 IU/ml) and streptomycin (10 mg/ml). Medium was replenished daily. Neural crest emigration was clearly apparent within 24 hours of culture. Cultures were subsequently flooded with 4% paraformaldehyde in PBS, fixed overnight at 4°C, and washed with PBS before photography and cell counting.

RESULTS

Bmp5 and *Bmp7* mRNA expression patterns overlap from gastrulation onwards

The localization of *Bmp7* transcripts at selected stages in the developing mouse embryo has been previously examined (Lyons et al., 1995; Arkell and Beddington, 1997; Dudley and Robertson, 1997; Furuta et al., 1997; Shimamura and Rubenstein, 1997; Solloway et al., 1998). Owing to the relative late-onset of defects in *se* mice, previous studies examining the localization of *Bmp5* have focused on late-gestation stage embryos (>13.5 dpc) (King et al., 1994; Solloway et al., 1998) or specific subsets of tissues (Dudley and Robertson, 1997; Furuta et al., 1997). To precisely define sites where Bmp5 and Bmp7 are coexpressed, we performed a comparative whole mount RNA in situ analysis on stage matched embryos from pre-streak (6.5 dpc) to 30 somites (10.5 dpc). *Bmp7* transcripts are first observed at the onset of gastrulation (early streak stage) within the distal primitive streak (Fig. 1B). This domain later expands to include the node and node-derived axial mesoderm. As gastrulation proceeds, mRNA is observed in the allantois as well as in the lateral mesoderm emerging from the primitive streak (Fig. 1D and data not shown). By the early headfold stage, mesodermal expression becomes restricted to the prospective heart and cranial mesoderm (Fig. 1D). *Bmp7* transcripts are detected in the dorsal neurectoderm at the early headfold stage, as well as throughout the surface ectoderm of the embryo (data not shown). By the 4-5 somite stage (8.0 dpc) expression extends throughout the heart tube and around the intraembryonic coelomic channel (Fig. 1F,H). In the cranial neural folds *Bmp7* mRNA becomes localized to the dorsal- and ventral-most aspects of the neurectoderm (Fig. 1H). *Bmp7* is also detected in the endoderm of the visceral yolk sac, and expression persists in the node, surface ectoderm and allantois (Fig. 1H and data not shown).

At 8.25-8.5 dpc, *Bmp7* expression persists in the most anterior dorsal neurectoderm, while expression in the cranial mesoderm extends caudally to the hindbrain (Fig. 1J,L). High levels of *Bmp7* transcripts are apparent in the ectodermal components of the optic vesicle, otic vesicle and branchial arches (Fig. 1J and data not shown). *Bmp7* mRNA becomes distributed throughout the endoderm of the foregut and hindgut pockets as they form and persists during gut tube closure (Fig. 1N). *Bmp7* expression in the heart becomes restricted to the developing myocardium and is undetectable in the endocardium (Fig. 1N). In addition, *Bmp7* is detected adjacent to the somites in the lateral plate mesoderm (Fig. 1P). After neural tube closure, *Bmp7* expression is seen in the dorsal neurectoderm (prospective roofplate), in a domain that extends along the length of the neural tube by the 20-25 somite stage (Fig. 2D). In addition to continued expression in the heart, branchial arches, otic and optic vesicles, visceral yolk sac and allantois, *Bmp7* transcripts are detected in the ectoderm and mesenchyme of the limb buds, surface ectoderm of the telencephalon and mesonephric ducts of the kidney (Fig. 2B,D). Similar results were obtained at 10.5 dpc (data not shown).

Interestingly, although we find that the domains of *Bmp5* and *Bmp7* expression are almost completely overlapping, *Bmp7* is usually expressed in a broader domain than *Bmp5*. Low levels of *Bmp5* transcripts are first observed in the presumptive anterior mesoderm shortly after initiation of gastrulation (Fig. 1A). Like *Bmp7*, this domain becomes restricted to the embryonic heart and cranial paraxial mesoderm (Fig. 1A,C). Low level expression is also detected in the allantois at this stage and in all subsequent stages examined (data not shown). At the early headfold stage, *Bmp5* mRNA appears in the dorsal aspect of the cranial neurectoderm as well as in the underlying mesenchyme (data not shown). By 8.0 dpc *Bmp5* is clearly expressed in the dorsal cranial neurectoderm and the subjacent cranial mesoderm (Fig. 1E,G). Expression also persists in the heart and coelomic channel. However, unlike *Bmp7*, *Bmp5* transcripts are not detectable in the gut endoderm, visceral yolk sac endoderm, ventral neurectoderm, or surface ectoderm at this stage (Fig. 1E,G).

This general pattern of expression is maintained at 8.25-8.5 dpc. *Bmp5* is highly expressed in the anterior-most dorsal neurectoderm and underlying mesenchyme with lower levels of expression extending caudally to the hindbrain (Fig. 1I,K). Increased *Bmp5* transcripts clearly delineate the midbrain-hindbrain sulcus (data not shown). Like *Bmp7*, *Bmp5* transcripts become localized to the heart myocardium, and expression extends caudally from the heart along the coelomic channels into the splanchnopleure and somatopleure components of the lateral plate mesoderm (Fig. 1I,M,O). At this time, *Bmp5* mRNA is also detected in the surface ectoderm overlying the branchial arches (Fig. 1I). Interestingly, in contrast to the ubiquitous ectodermal expression of *Bmp7*, *Bmp5* transcripts are localized to the distal tips of the arches (Fig. 2A). *Bmp5* mRNA is still present in the heart, arches and allantois at 9.5 dpc (Fig. 2B). Expression persists in the lateral plate mesoderm immediately caudal to the forelimb bud. Transcripts are also observed in the caudal-most mesoderm of the bud (data not shown). Transcription in the dorsal neurectoderm becomes limited to two stripes of expression abutting the midline of the dorsal telencephalon in a domain extending caudally from the commissural plate of the telencephalon to the midbrain-forebrain isthmus.

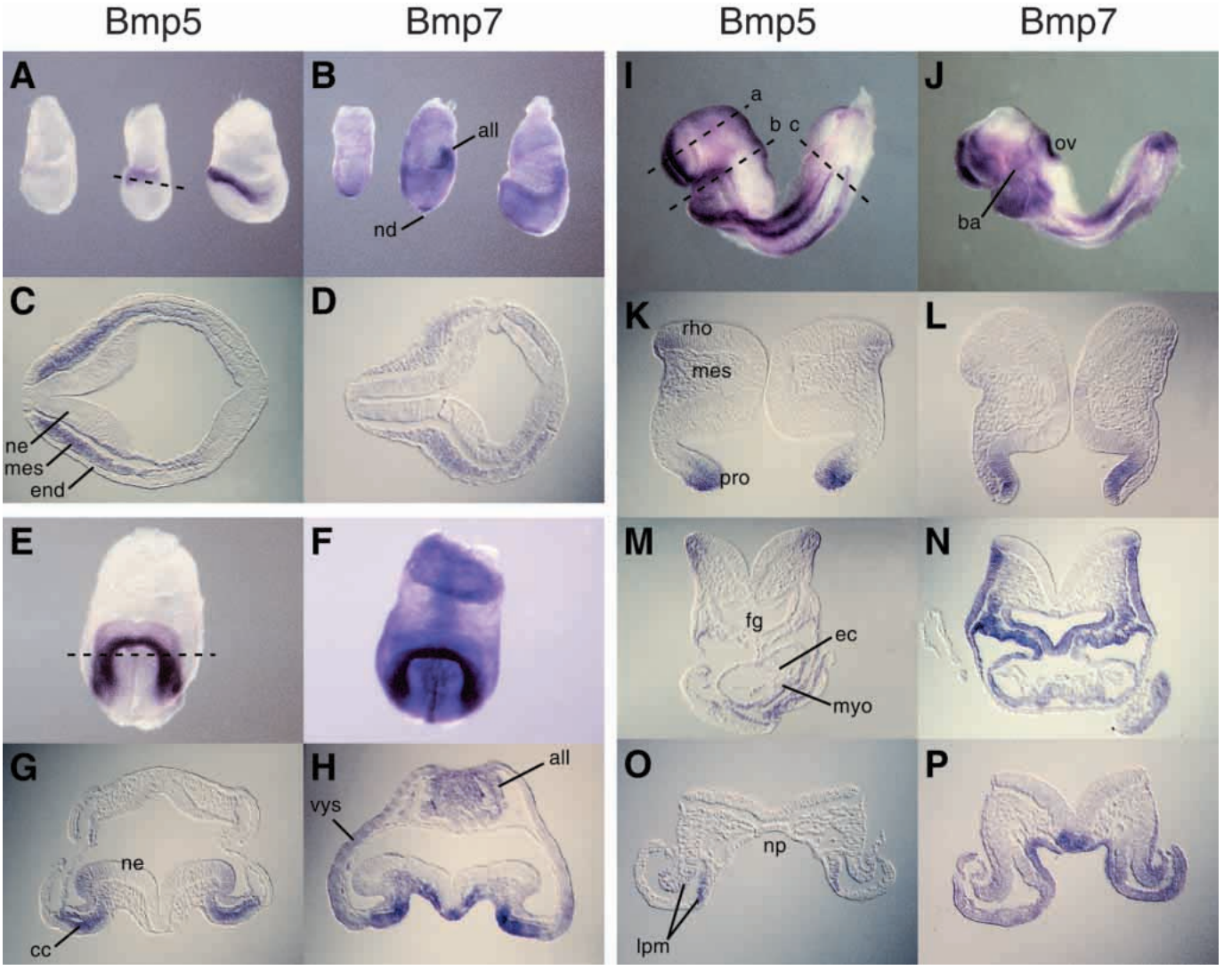

Fig. 1. Comparison of *Bmp5* and *Bmp7* expression in mouse embryos from 6.5 to 8.5 dpc by whole-mount in situ hybridization. Transverse sections (C,D,G,H, and K-P) correspond to regions in A, E, and I marked by a dotted line. (A,B) Lateral views and (C,D) sections of gastrulation stage embryos (6.5-7.5 dpc). *Bmp5* transcripts are first observed in anterior mesoderm (A,C), whereas *Bmp7* is more broadly expressed in the embryonic and extraembryonic mesoderm, anterior primitive streak, and node (B,D). (E,F) Frontal views and (G,H) sections of 4-5 somite (8. 0 dpc) embryos. *Bmp5* and *Bmp7* are coexpressed in the heart, allantois, and anterior dorsal neurectoderm and mesoderm. (H) *Bmp7* is also expressed in the yolk sac endoderm and ventral neurectoderm. (I-P) 10 somite (8.5 dpc) embryos; lateral view. Sections in K,L, M,N, and O,P correspond to a, b, and c in I, respectively. (I) *Bmp5* is expressed in the branchial arch ectoderm and distal tip of the tailbud, (I,K,M) dorsal rostral neurectoderm, (K,M) underlying mesenchyme, and (M) heart. (I,O) *Bmp5* transcripts are also present in the lateral plate mesoderm and allantois (data not shown). (J,L,N,P) In addition to being expressed similarly to *Bmp5*, *Bmp7* is expressed in the otic vesicle (J), foregut endoderm (N), and notochordal plate (P). all, allantois; nd, node; ne, neurectoderm; mes, mesoderm; end, endoderm; cc, coelomic channel; vys, visceral yolk sac endoderm; ov, otic vesicle; ba, branchial arch; rho, rhombencephalon (prospective hindbrain); pro, prosencephalon (prospective forebrain); fg, foregut; ec, endocardium; myo, myocardium; lpm, splanchnopleure and somatopleure components of lateral plate mesoderm; np, notochordal plate.

We found only one tissue that expresses *Bmp5* in the absence of *Bmp7*. In 8-10 somite embryos (8.5 dpc) low levels of *Bmp5* transcripts accumulate in the ventral quadrant of a subset of epithelial somites (Fig. 2A,E,F). This expression domain is first detectable in the fifth somite rostral to the tailbud (Fig. 2E). In 9.0 dpc (15 somite) embryos *Bmp5* mRNA persists from the fifth to the twelfth somite (Fig. 2G). Increased transcript levels are detected at the rostral and caudal boundaries of each somite, whereas expression rapidly tapers off in the older (i.e. more rostral) somites. Low levels of *Bmp5* expression are maintained in the somites at 9.5 dpc (Fig. 2C).

Early onset defects in *Bmp5; Bmp7* double mutants

We generated double mutant embryos lacking Bmp5 and Bmp7 to test whether these molecules can functionally compensate for each other during development. Outbred $Bmp7^{m1Rob}$ heterozygotes (Dudley et al., 1995) were bred to se^{GnJ} homozygotes (Green, 1942). F_1 double heterozygotes were then intercrossed to generate nine different combinations of

alleles at the *Bmp5* and *Bmp7* loci (animals wild type, heterozygous, or homozygous for mutations in either of the two genes). No double mutants were recovered from over 500 newborn F_2 progeny.

To determine the onset of embryonic lethality in *Bmp5;Bmp7* double mutants we initially examined 10.5 dpc embryos from double heterozygous intercrosses (Table 1). Out of a total of 89 embryos, 10 double mutants were recovered. These embryos were approximately 2/3 the size of littermates, and showed severe developmental defects in the rostral neural tube, allantois, heart, branchial arches, ventral body wall, and somites (Fig. 3D,E). In addition, double mutants displayed a weakened or absent heartbeat and pooled blood in the yolk sac. Despite these defects, *Bmp5;Bmp7* mutants did not display an overall delay in development, and in most cases the embryos contained the same number of somite pairs as controls. Histological analysis also revealed signs of cell necrosis in 50% of these embryos. Accordingly, all embryos were subsequently collected at timepoints prior to 10.5 dpc.

Progeny from timed matings between *se/se; Bmp7/+* intercrosses were analyzed for gross abnormalities related to those observed at 10.5 dpc. 7.5 dpc mutants were morphologically indistinguishable from littermates (data not shown). At 8.5 dpc, the open neural folds of normal embryos initiate fusion along the cranial midline at multiple sites, including the fore/midbrain boundary and the anterior extremity of the forebrain (Geelen and Langman, 1977). In contrast, the cranial neural folds in *Bmp5;Bmp7*-null embryos fail to elevate and approach each other (Fig. 3A). By 9.5 dpc, the cranial neuroepithelium has completely fused in normal embryos (Fig. 3B), but remains open in double mutants from the hindbrain rostrally to the anterior extremity of the forebrain (Fig. 3C). By 10.5 dpc, however, the majority of double mutants had initiated closure of the hindbrain and forebrain neuroepithelia, but the hindbrain roofplate was disproportionately reduced in size (Fig. 3E). In all cases the junction between the hindbrain roofplate and neuroepithelium was abnormally kinked and thickened, and kinks were observed along the length of the neural tube.

Interestingly, fusion of the allantois to the chorion was severely affected in *Bmp5;Bmp7* double mutants (Table 1). At 8.5 dpc the allantois forms a connection to the rudimentary placenta by fusion with the chorion. 74% of control embryos had established chorio-allantoic fusion by 8.5 dpc, in comparison to 40% of the double mutants. Furthermore, although chorio-allantoic fusion is normally complete by 9.5 dpc, only 2/3 of *Bmp5;Bmp7*-null embryos had fused by this timepoint. In the majority of these cases, the association between the allantois and chorion was poorly established, allowing easy separation of the two tissues during dissection. Very few double mutants maintained contact with the placenta at 10.5 dpc, and none of these embryos displayed the distinctive funnel-shaped allantois of their control littermates. Instead, double mutant allantoises were smaller and appeared to be slightly constricted at the base (Fig. 3A).

Heart development was noticeably retarded in *Bmp5;Bmp7* double mutants (Table 1). Double mutants form a normal primitive heart tube at 8.0 dpc. By 8.5 dpc normal embryos had begun to form separate ventricles, whereas the majority of double mutants were still in the initial stages of heart looping (Fig. 3A). This delay in heart development was more pronounced at 9.5 dpc and 10.5 dpc, but was difficult to characterize by gross morphology. Heart function was severely compromised in older embryos and this defect is likely responsible for embryonic lethality around 10.5 dpc.

Three additional defects are apparent in 9.5 dpc *Bmp5; Bmp7* double mutants. We found that ventral closure was delayed in many double mutants at 9.5 dpc, and the lateral plate often failed to fold ventrally towards the midline (Fig. 3C). Branchial arch outgrowth was also dramatically reduced in all *Bmp5;Bmp7* mutants examined. The first branchial arch was smaller in 9.5

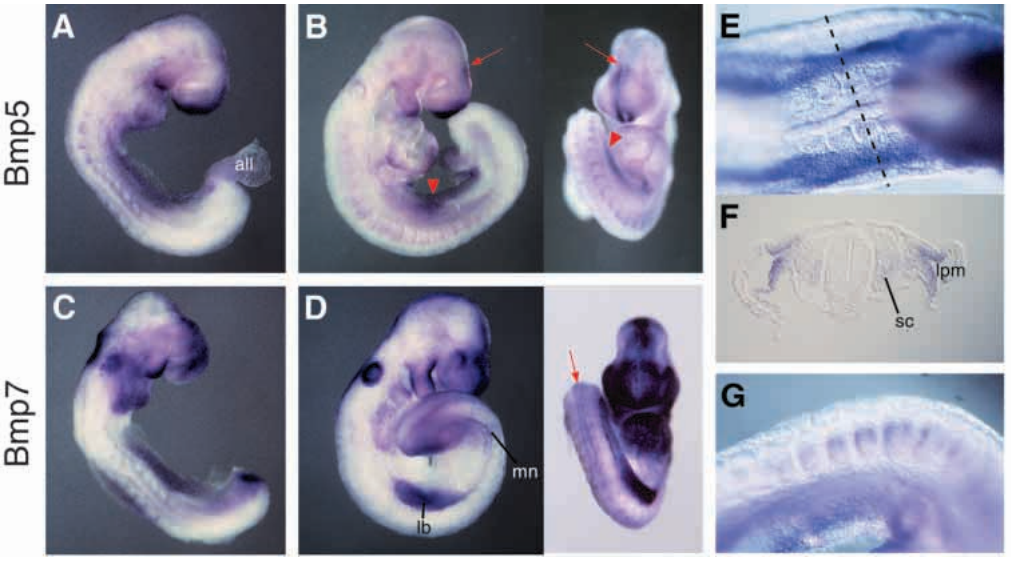

Fig. 2. Expression of *Bmp5* and *Bmp7* at later somite stages. (A,B,E-G) *Bmp5*, (C,D) *Bmp7*; (E,F) 10 somites, (A,C,G) 15 somites (B,D) 20 somites. (A) *Bmp5* expression decreases in the hindbrain at 9.0 dpc. Transcripts are present in the heart, rostral (older) somites, lateral plate mesoderm, allantois (all), branchial arches, and rostral neurectoderm. (B) Two stripes of *Bmp5* expression mark the dorsal forebrain neurectoderm in older embryos. Note the reduction in expression at the forebrain/midbrain sulcus (arrows). Previous sites of *Bmp5* expression, including the lateral plate mesoderm (arrowhead) and somites, are preserved. (C,D) *Bmp7* transcripts are never detected in the somites at any stages examined. (D) At 9.5 dpc *Bmp7* transcripts are broadly expressed at all sites of *Bmp5* expression except in the somites. New sites of expression include the mesonephros (mn), forelimb bud ectoderm (lb), and the length of the dorsal neural tube (arrow). (E) Dorsal view at 10 somite stage. Anterior is to the right. *Bmp5* transcripts first appear in the fifth somite rostral to the tailbud. (F) Transverse section corresponding to the dotted line in (E). *Bmp5* transcripts are present in the sclerotome (sc) of the somites and lateral plate mesoderm (lpm). (G) Close-up, lateral view of *Bmp5* expression in a 15 somite embryo. Note the higher level expression in the rostral and caudal aspects of each somite, as well as the overall increase in expression in more mature somites.

Table 1. Onset and penetrance of phenotype in *Bmp5;Bmp7* double mutants

Collection time	Embryos	Mutants (%)	Chorioallantoic fusion		Reduced branchial arch growth (%)	Retarded heart growth (%)	Unfused rostral neural tube (%)
			Controls (%)	Mutants (%)			
8.5 dpc	136	32 (24%)	77/104 74%)	13/32 (40%)	N/A	N/A	N/A
9.5 dpc	114	34 (30%)	79/80 (99%)	22/34* (65%)	34/34 (100%)	34/34 (100%)	34/34 (100%)
10.5 dpc‡	107	17	90/90	6/17§	17/17 (100%)	17/17 (100%)	14/17 (82%)

N/A, not assessed

*Of 22 double mutants that had chorioallantoic fusion at 9.5 dpc, 17 (77%) displayed a very loose association between the allantois and the chorion which was easily broken during dissection. In contrast, all of the control embryos at this stage maintained a tight junction between these two tissues.

‡All data was collected from s*e/se*; *Bmp7*/+ intercrosses with the exception of the 10.5 dpc collections which also included progeny from double heterozygous intercrosses. 10 double mutants were recovered out of 89 total progeny from double heterozygous intercrosses, but observation of the heartbeat indicated that most of these animals were dead or dying.

§Most double mutants were developmentally retarded by 10.5 dpc and exhibited edema of the ventral body wall.

dpc double mutant embryos compared to similarly staged, normal littermates. All three branchial arches were discernible by 10.5 dpc, but their size was significantly reduced in relation to the overall size of the mutant embryos. Finally, we note that at 10.0-10.5 dpc double mutants often displayed abnormalities in somite morphogenesis. The somites were closely packed together, and a subset of somites caudal to the forelimb were often fragmented and unevenly shaped (Fig. 3E).

Abnormal patterns of apoptosis in *Bmp5; Bmp7* mutants

One potential mechanism underlying many features of the double mutant phenotype, including the reduced size of the forebrain and branchial arches and the somite abnormalities, could be abnormal apoptosis. We performed whole-mount TUNEL labeling on control (n=10) and double mutant (n=6) littermates at 9.5-10.0 dpc. All embryos, regardless of genotype, displayed identical patterns of apoptotic cells in the nasal placodes and limb buds (Fig. 4A,E). Normally, a large population of cells along the dorsal midline undergoes apoptosis after neural tube closure (Schlüter, 1973). Intriguingly, fewer apoptotic cells were observed along the length of the dorsal midline of double mutant embryos compared to controls (Fig. 4B,F) containing the same number of somites. Two 10.0 dpc mutants with partial neural tube closure had no TUNEL-positive cells in this region, indicating that the reduced cell death is not due to a developmental delay. Two severely affected double mutants showed diffuse, generalized staining, and section analysis revealed obvious signs of cell necrosis (data not shown). Three of the remaining four mutant embryos had increased staining in the dermomyotome of the somites caudal to the forelimb bud in precise correspondence to the regions of somite abnormalities (Fig. 4G and data not shown). However, a reiterated pattern of somitic cell death normally occurs during vertebrate development (Jeffs and Osmond, 1992) and was observed in some control embryos (Fig. 4C). Additionally, dying cells were rarely observed in the first branchial arch in controls (Fig. 4D), but all double mutant embryos showed extensive TUNEL-positive cells in the surface ectoderm at the base of the first

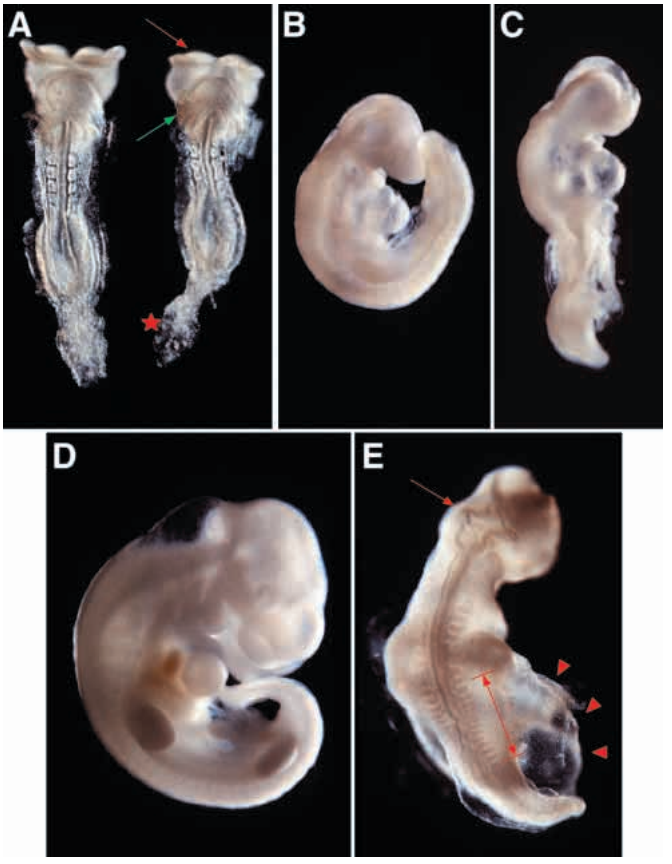

Fig. 3. Phenotypic abnormalities in *Bmp5;Bmp7* double mutant embryos. Allantoises were removed in B-D. (A) 8.5 dpc; (B,C) 9.5 dpc; (D,E) 10.5 dpc. (A) Double mutant embryos (right) first become morphologically distinct from control littermates (left) at 8.5 dpc. Note the abnormal development of the cranial neural folds (red arrow), heart (green arrow), and allantois (star). Both embryos are at the 8 somite stage. (B) Normal 9.5 dpc embryo. (C) *Bmp5;Bmp7* double mutant embryo; defects are apparent in the cranial neural folds, branchial arches and heart. In addition, the embryo has not yet turned. (D) Normal 10.5 dpc embryo. (E) Dorsal view of a severely affected double mutant at 10.5 dpc. In addition to the defects observed at 9.5 dpc, these embryos display fragmented somites (bracketed arrow) and abnormal edema of the ventral body wall (arrowheads). The hindbrain roofplate is also reduced in size and abnormally thick (arrow).

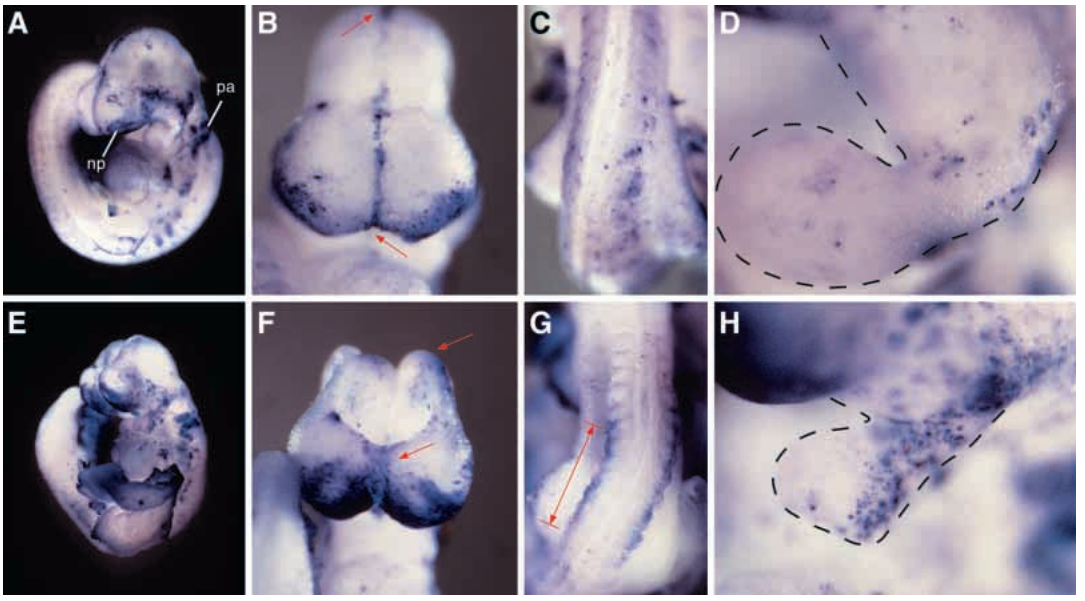

Fig. 4. Apoptotic cell death in wild-type and double mutant embryos at 9.5 dpc as revealed by whole-mount TUNEL. (A-D) Normal embryo. (E-F) *Bmp5;Bmp7* double mutant embryo. (A) Apoptotic cells are observed in the dorsal midline, pharyngeal arches (pa), nasal placode (np), and limb bud. (B) Labeled cells are present in the dorsal midline of both the forebrain and midbrain (region between arrows). (C) Scattered apoptotic cells are present in the somites at the level of the forelimbs. (D) Close-up view of the first branchial arch (outlined) showing few dying cells. (E) Similar patterns of apoptosis are observed in the nasal placodes, limb buds (data not shown), and pharyngeal arches of double mutant embryos. (F) Few apoptotic cells are present in the dorsal midline of the forebrain and midbrain. (G) Apoptotic cells are present in the mediolateral dermomyotome of the seven somites overlying and caudal to the forelimb bud (bracketed). Note the correspondence to other regions of somite patterning anomalies (see Fig. 9). (H) Increased apoptosis is observed throughout the ectoderm at the base of the first branchial arch. (A,E; B,F; C,G; D,H, same magnification).

arch (Fig. 4H). Collectively these data suggest that abnormal patterns of cell death may contribute to the defects in somitogenesis, branchial arch growth, and neural tube closure.

Abnormal development of the rostral neuroepithelium

BMP molecules have previously been implicated in the differentiation of the dorsal neural tube (Liem et al., 1995). To determine whether the loss of Bmp5 and Bmp7 modifies the identity of the neural tube, we examined the expression of several regionally restricted neuroepithelial markers. *Shh* was used as a ventral CNS marker. In 8.5 dpc (8 somites) and 9.5 dpc (25 somites) embryos *Shh* is expressed in the ventral midline of the brain and rostral spinal cord, as well as in the node, notochord, and foregut and hindgut endoderm (Fig. 5A; Echelard et al., 1993). Normal patterns of *Shh* expression were consistently observed in *Bmp5;Bmp7* double mutants (Fig. 5B), suggesting that the ventral midline and gut were correctly specified.

Wnt-1 expression was used to evaluate development of the dorsal CNS (Parr et al., 1993). The general domains of *Wnt-1* expression were identical between double mutant and control embryos at 8.5 dpc. However, examination of older mutant embryos uncovered several interesting results. At 9.5 dpc, despite the failure of neural tube closure, *Wnt-1* transcripts are correctly localized to the dorsal midbrain and along the midbrain/hindbrain boundary (Fig. 5C). Thus, the basic anterior/posterior and dorsal/ventral boundaries of the brain are correctly specified in mice lacking both Bmp5 and Bmp7. *Wnt-1* transcripts in the dorsal metencephalon also reveal a striking reduction in the size of the mutant hindbrain roofplate at 10.5 dpc in comparison to control littermates (Fig. 5G,H). Interestingly, ectopic expression of Bmp7 in the hindbrain causes dorsalization and expansion of adjacent neurectoderm (Arkell and Beddington, 1997). The growth of the lobes of the forebrain (telencephalon) is also severely compromised in *Bmp5;Bmp7* mutants. Thus the distance between the nasal placodes and the rostral extent of *Wnt-1* expression in the midbrain is reduced in 9.5 dpc embryos (Fig. 5C), and this phenotype increases in severity by 10.5 dpc (data not shown). These affected areas correlate remarkably well with the overlapping expression of *Bmp5* and *Bmp7* in the early hindbrain (8.5 dpc) and dorsal telencephalon (8.5-10.5 dpc) (Fig. 1; Furuta et al., 1997).

To more clearly delineate the defects in the rostral CNS, we assessed the expression of *Fgf-8* and *Wnt-8b* during development of the forebrain. *Fgf-8* transcripts are localized to the mid/hindbrain isthmus and the rostral neural plate in 8.5 dpc control embryos. Expression is also observed in the tailbud and the splanchnic mesoderm of the intraembryonic coelom. *Fgf-8* expression was unperturbed in double mutants at this stage (data not shown). By 10.5 dpc, *Fgf-8* mRNA is also apparent in the pharyngeal pouches, AER of the limb buds, mid/forebrain boundary (zona limitans), commissural plate of the forebrain, surface ectoderm of the first branchial arch, and in a subpopulation of the lateral myotome located at the rostral and caudal margins of each somite (Fig. 5D; Heikinheimo et al., 1994). Analysis of two double mutant embryos at 10.5 dpc reveals normal distribution of *Fgf-8* transcripts in the pharyngeal pouches, branchial arches, AER, and mid/hindbrain constriction despite their reduced size in comparison to controls (Fig. 5D). However, *Fgf-8* expression patterns are perturbed at three sites. First, *Fgf-8* expression highlights a disproportionate reduction in the growth of the maxillary and mandibular components of the first branchial arch. Second, myotomal expression of *Fgf-8* observed in the somites of control embryos is absent in *Bmp5;Bmp7* double mutants at 10.5 dpc (see below). Finally, the domain of *Fgf-8*

expression in the commissural plate of the telencephalon, indicative of the ventral- and rostral-most portion of the forebrain, is positioned abnormally close to the mid/forebrain isthmus. The apparent reduction in the caudal aspect of the telencephalon in double mutants was confirmed by analysis of *Wnt-8b* expression (Fig. 5E,F). *Wnt-8b* marks the dorsal region of the telencephalon and expression extends caudally into the diencephalon at 10.5 dpc (S. Lee and A. McMahon, personal communication). In keeping with the *Wnt-1* and *Fgf-8* results, all 4 double mutants analyzed at 9.5 dpc showed a drastic reduction in the rostral extent of *Wnt-8b* expression in the forebrain (Fig. 5F). We conclude that Bmp5 and Bmp7 play a regulatory role in the growth of the telencephalon and metencephalon.

Failure of chorioallantoic fusion in double mutants

Bmp5 and *Bmp7* are coexpressed in the allantois throughout its development (Figs 1 and 2), and normal chorioallantoic fusion rarely occurs in *Bmp5;Bmp7* double mutants (Table 1). This defect could possibly be due to reduced cellular proliferation, abnormal morphogenesis, or aberrant adhesion in the allantois. Histological analysis of 9.5 dpc mutants and controls reveal abnormalities in the progression of fusion between the allantois and chorion. In control littermates (n=3) the allantoic mesoderm was distributed over the entire chorionic surface and was extensively invading the trophoblast (Fig. 6G). Although the allantois and chorion were touching in double mutants (n=3), the allantois was associated with only part of the chorionic membrane (Fig. 6H). Despite this, double mutant allantoises appeared morphologically normal and contained vacuolated mesenchyme, vasculature, and red blood cells (Fig. 6H and data not shown). Invasion of the placental trophoblast layer was also seriously reduced. This phenotype is highly reminiscent of defects observed in embryos lacking the transmembrane glycoprotein VCAM-1 (Gurtner et al., 1995; Kwee et al., 1995) or its cognate receptors, the α_4 integrins (Yang et al., 1995). High levels of VCAM-1 protein are present in the distal allantois, and α_4 integrin is distributed throughout the chorionic epithelium. It is tempting to speculate that the absence of Bmp5 and Bmp7 prevents the appropriate specification of a subset of mesoderm cells necessary for the growth and adhesion of the allantois to the chorion.

mTwist expression is also highly abnormal within the allantois of double mutants. *mTwist* transcripts are normally localized throughout the extraembryonic mesoderm as it exits the primitive streak and enters the allantois (Fig. 6A, top embryo). However, in double mutants examined at either 8.5 or 9.5 dpc *mTwist* expression was confined to a 'sheath' of cells at the base of the primitive streak which surrounded a core of *mTwist*-negative mesoderm (Fig. 6A, bottom embryo). In addition, the expression levels of *mTwist* rapidly diminished at the distal tip of the allantois. These data indicate that Bmp5

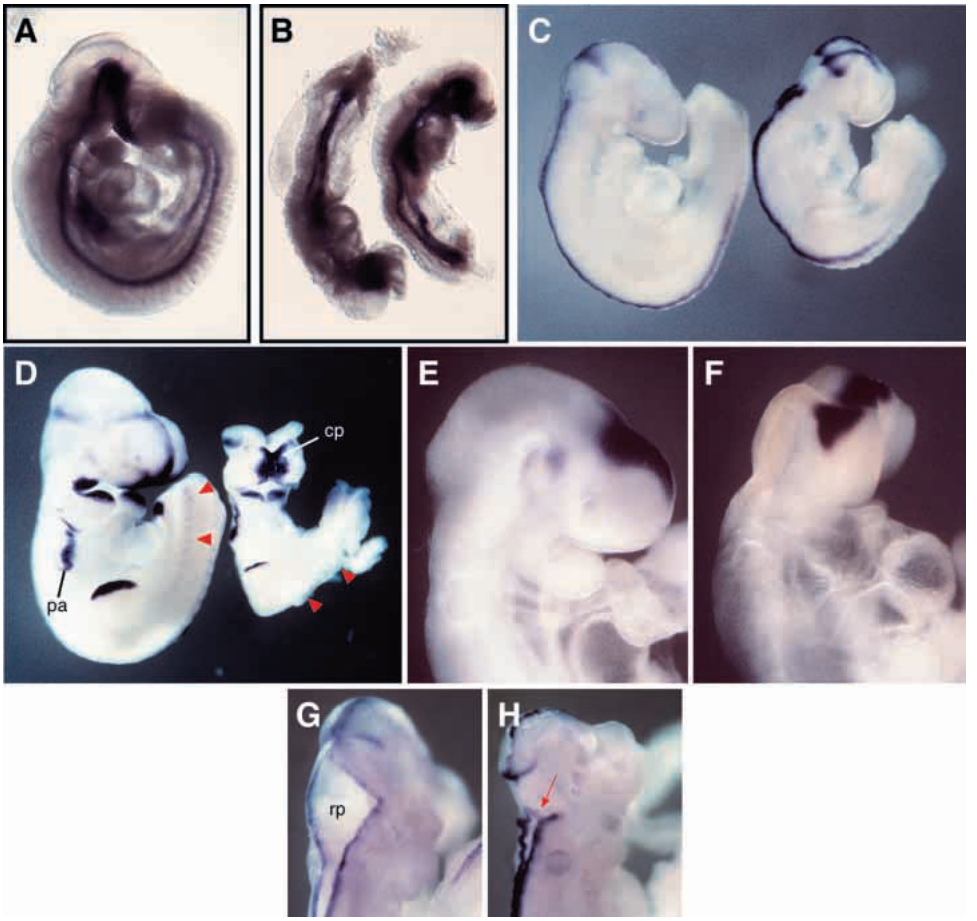

Fig. 5. Expression of CNS markers in wild-type (leftmost) and mutant embryos. (A-C,E,F) 9.5 dpc; (D,G,H) 10.5 dpc. (A) Wild-type *Shh* expression. (B) Normal expression of *Shh* in the floorplate and gut of *Bmp5;Bmp7* mutants. (C) The expression of *Wnt-1* along the midline and in the dorsal midbrain is unaffected by the lack of rostral neural tube closure in double mutants (right). However, note the reduction of neurectoderm rostral to the midbrain/forebrain boundary in the double mutant embryo. (D) Similar *Fgf-8* expression is observed in the branchial arches, pharyngeal arches, AER, commissural plate, and midbrain boundaries of wild-type and *Bmp5;Bmp7* mutants. Note the reduction in myotomal expression (arrowheads) and the abnormal positioning of the commissural plate in the double mutant. (E) *Wnt-8b* expression in the dorsal telencephalon and diencephalon at 9.5 dpc. (F) The *Wnt-8b* expression domain is markedly reduced in *Bmp5;Bmp7* mutants. (G) By 10.5 dpc, *Wnt-1* expression delineates the dorsal midbrain, midbrain/hindbrain isthmus, and the edges of the hindbrain roofplate. (H) *Wnt-1* expression in a double mutant littermate; the hindbrain roofplate (arrow) is severely reduced in size. Although the midbrain has closed, the forebrain remains open in this mutant (data not shown). cp, commissural plate; pa, pharyngeal arch; rp, hindbrain roofplate.

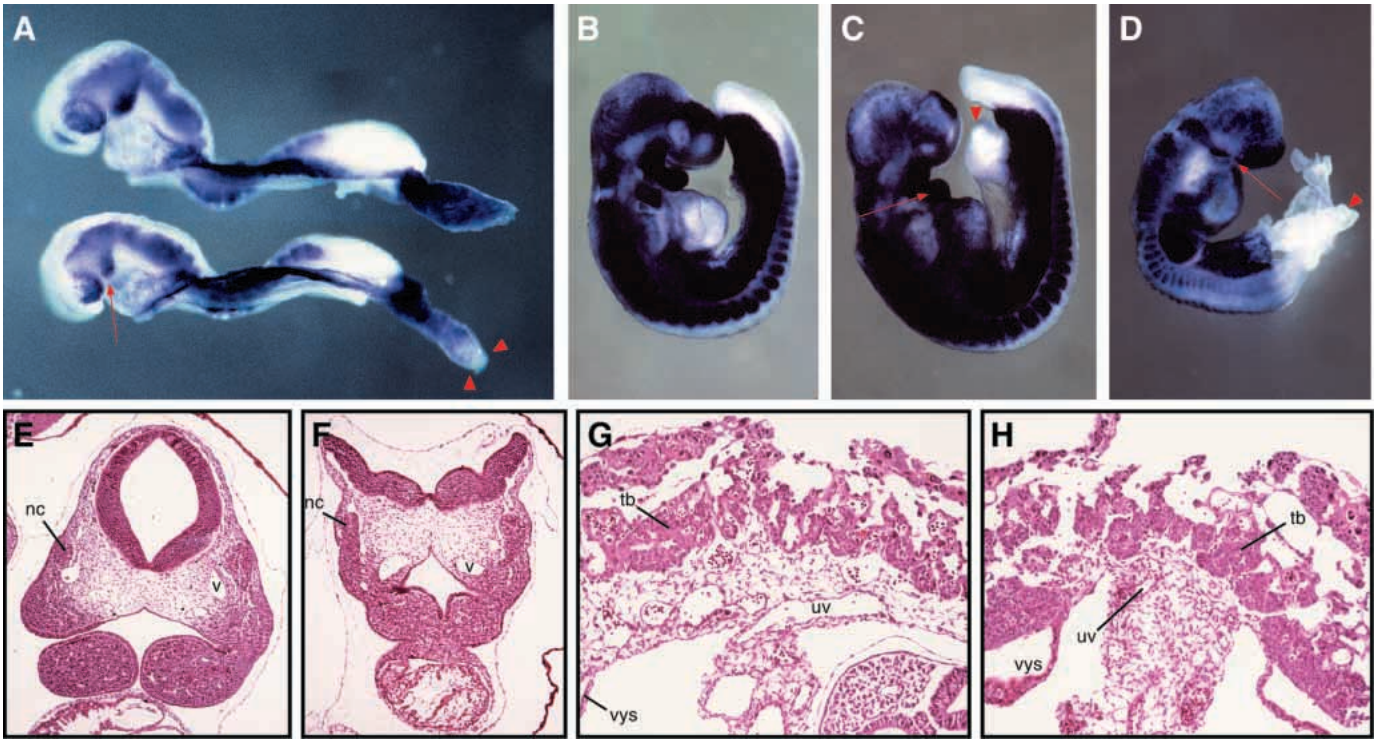

Fig. 6. Development of the branchial arches and allantois is compromised in *Bmp5;Bmp7* mutants. (A-D) *Twist* expression at 8.5 dpc (A) and 9.5 dpc (B-D). (A) A reduction in *Twist*-positive mesenchyme is apparent in the head, branchial arches (arrow) and distal allantois (arrowheads) of the double mutant (lower) embryo in comparison to a normal littermate. Both embryos are at the 10 somite stage. (B) Wild-type *Twist* expression. (C) Less severely and (D) more severely affected *Bmp5;Bmp7* embryos continue to show a delay in branchial arch growth (arrows) and an abnormal reduction in *Twist* expression in the allantois (arrowhead). Chorioallantoic fusion failed to occur for both embryos. (E-H) Histological analysis of wild-type and *Bmp5;Bmp7* embryos at 9.5 dpc. (E) Transverse sections through wild-type and (F) double mutant first branchial arches. In the *Bmp5;Bmp7* embryo the neural folds remain open and branchial arches are reduced in size despite the influx of neural crest. (G) Section through a wild-type placenta shows allantoic mesoderm spread over the entire placental region. Umbilical vessels are apparent and allantoic mesoderm is invading the trophoblast extensively. (H) The placenta from a double mutant is reduced in size. Allantoic mesoderm is not evenly distributed over the placenta and trophoblast invasion is reduced. Umbilical vessels are present. nc, trigeminal neural crest; v, vein; uv, umbilical vessels; tb, trophoblast; vys, visceral yolk sac.

and Bmp7 may be involved in the maturation of the allantois and the formation of a normal chorioallantoic boundary.

Branchial arch development is compromised in *Bmp5;Bmp7* double mutants

The growth of the branchial arches is severely compromised in 9.5 dpc and 10.5 dpc mutants (Fig. 6E,F). The branchial arches are derived from pharyngeal endoderm, surface ectoderm, paraxial mesoderm, and neural crest cells, although little is known about the interactions between these different tissues which guide morphogenesis. *Bmp5* and *Bmp7* are expressed in the dorsal cranial neurectoderm and mesenchyme from early headfold stages onwards (Fig. 1), as well as in the surface ectoderm of the branchial arches from their earliest formation (Fig. 2 and data not shown), suggesting that *Bmp5* and *Bmp7* signaling could affect branchial arch growth by influencing the neural crest, mesenchyme, and/or ectoderm components of the arches.

To address whether there is a failure of the mesenchymal core of cells to migrate into the arches and proliferate, we compared *mTwist* expression in double mutants and wild-type embryos. *mTwist* has been implicated in regulating the morphology and behavior of head mesenchyme cells (Chen and Behringer, 1995) and is expressed in a large number of mesodermally derived tissues (Füchtbauer, 1995). At 8.5 dpc, *mTwist* is expressed in the mesenchymal cells of the head and branchial arches (Fig. 6A, top embryo). Additional areas of expression include the somatopleura of the lateral plate, the allantois, and the somites. The domain of *mTwist*-positive mesenchymal cells in the head and branchial arches was reduced in *Bmp5;Bmp7* double mutants in comparison to controls compared at 10-, 15-, and 25 somite stages (Fig. 6A-D and data not shown). These results suggest that the lack of branchial arch growth in the mutants may be in part due to the abnormal development of the contributing mesenchyme cells.

Trunk neural crest are reduced in *Bmp5; Bmp7* mutants

Neural crest cells also contribute to the growth of the branchial arches. At 8.5 dpc (12 somites), control embryos showed intense staining of the neural crest-specific marker *AP-2* (Mitchell et al., 1991) along the dorsal aspect of the neural folds from the hindbrain rostrally (Fig. 7A). A similar pattern was observed in the double mutants, but the level of *AP-2* expression was markedly reduced in the rostral-most aspect of the neurectoderm near the midline and corresponding to the

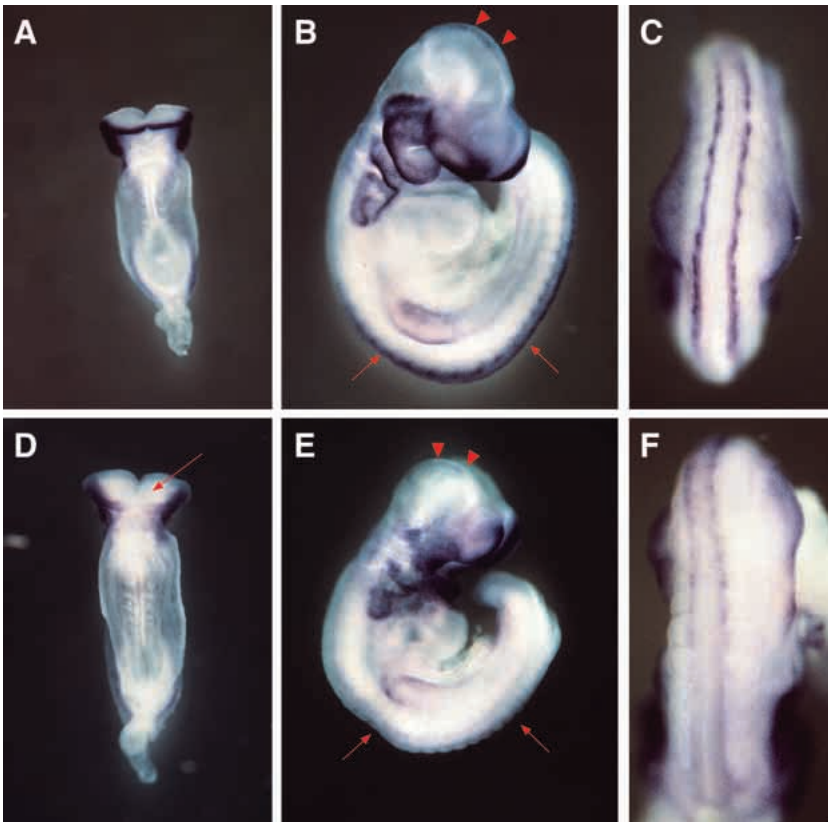

Fig. 7. Expression of *AP-2* in *Bmp5;Bmp7* embryos. (A,D) *AP-2* expression in 8.5 dpc and (B,C,E,F) 9. 5 dpc embryos. (A) Wild-type expression of *AP-2* in the dorsal cranial neural folds at 8.5 dpc. (B) *AP-2* expression in the neural crest-derived mesenchyme of the face and arches at 9.5 dpc. Transcripts are also present in the trunk ganglia (arrows), midbrain (arrowheads) and limb buds. (C) Higher magnification dorsal view of trunk ganglia near the forelimb bud. (D) *AP-2* expression is reduced in the rostral neurectoderm of 8.5 dpc double mutants (arrow). (E) *AP-2*-positive cells can colonize mutant craniofacial mesenchyme and arches at 9.5 dpc. Despite being expressed in the limb bud and midbrain (arrowheads), *AP-2* transcripts are reduced in the trunk (arrows). (F) Comparable view to C demonstrating the severe loss of *AP-2* expression in the trunk.

region where *Bmp5* and *Bmp7* are normally strongly coexpressed (Fig. 7D). By 9.5 dpc (25 somites), we observe *AP-2* transcripts in the neural crest-derived craniofacial mesenchyme, cranial ganglia, dorsal root ganglia, and branchial arch mesenchyme of control and double mutant embryos (Fig. 7B,E). Collectively these data suggest that cranial neural crest cells are able to develop and migrate in the absence of Bmp5 and Bmp7 signaling. The expression of *AP-2* in the telencephalon also highlights the reduction in growth of this structure in *Bmp5;Bmp7* double mutants (Fig. 7E).

Surprisingly, the expression of *AP-2* in the trunk ganglia was almost completely abolished in the double mutants (Fig. 7C,F), raising the possibility that neural crest cell precursors in the neural tube die or fail to develop in the absence of Bmp5 and Bmp7. *Bmp7* is expressed in the roofplate of the neural tube and overlying ectoderm (Lyons et al., 1995; Arkell and Beddington, 1997; Dudley and Robertson, 1997; Furuta et al., 1997) and can induce the differentiation of dorsal cells and neural crest in the neural tube (Liem et al., 1995). Moreover, expression of *Bmp5* mRNA in the somites could potentially influence the differentiation of the neural tube or neural crest. We used a tissue culture assay to examine the differentiation and emigration of neural crest from wild-type and double mutant neural tube explants obtained at 9.5 dpc (Stemple and Anderson, 1992). In both cases, neural crest cell emigration was readily apparent 24 hours after culture. Neural crest cells from *Bmp5; Bmp7* double mutants were morphologically identical to control cells and were present at similar densities on the culture plates over a five day culture period (data not shown). Thus, the neural crest precursor cell pool appears unaffected in the double mutant embryos. However, this assay cannot exclude the possibility that Bmp5 and Bmp7 are involved in the subsequent proliferation, migration, and differentiation of these cells in the intact embryo.

Heart morphogenesis is delayed in *Bmp5; Bmp7* mutants

Early in cardiac development (approx. 7.0 dpc), bilaterally symmetric populations of anterior mesoderm adjacent to the headfolds become specified to a cardiogenic fate by diffusible factors from the adjacent endoderm. These cells then migrate medially and fuse to form a primitive heart tube composed of inner endocardial cell layers and outer myocardial layers. A stereotyped program of looping and septation subsequently generates the mature four-chambered heart (for reviews see Fishman and Chien, 1997). *Bmp5* and *Bmp7* are coexpressed in the anterior mesoderm during the initial specification of cardiac cells at 7.0 dpc, and they continue to be broadly expressed throughout the heart myocardium until at least 10.5 dpc, the latest stage examined. In keeping with this expression pattern, a general delay in the development of the heart was consistently observed in *Bmp5; Bmp7* double mutant embryos (Table 1).

MLC2A transcripts are present throughout the early heart, becoming atrially restricted at 9.0 dpc (Kubalak et al., 1994). At 8.5 dpc (10 somites), control embryos are in the process of early heart chamber formation (Fig. 8A,C). The myocardial and endocardial cell layers are apparent, and the bulbus cordis (future right ventricle) is morphologically distinct from the presumptive left ventricle. In contrast, *MLC2A* expression shows that double mutants consistently exhibit a delay in heart morphogenesis with the heart of a 10 somite double mutant

more closely resembling that of control embryos at the 6-8 somite stage (Fig. 8B,D). This was further corroborated by histological analysis of 8 control and 7 double mutant embryos at 8.5 dpc (data not shown). By 9.5 dpc the majority of double mutants (4/5) had initiated heart looping morphogenesis and had formed the atrial and ventricular chambers. Although chamber septation had occurred in these embryos, the general morphology of the heart was disorganized (Fig. 8F). The myocardial walls of each chamber were often abnormally kinked and ruffled, and the pericardium was noticeably thickened. All control embryos at 9.5 dpc (n=5) had formed the common atrium and ventricle. Heart morphology was invariant between controls and no ruffling of the chamber walls was observed (Fig. 8E). Analysis of viable 10.5 dpc mutant embryos showed that, in contrast to controls (Fig. 8G), chamber septation had failed to occur (Fig. 8H). Overall cell density and trabeculation was reduced in the mutant myocardia. Notably, the endocardial cushions, the anlage of the future heart valves, were missing in these double mutants although this may be due to the overall delay in the growth and differentiation of the heart.

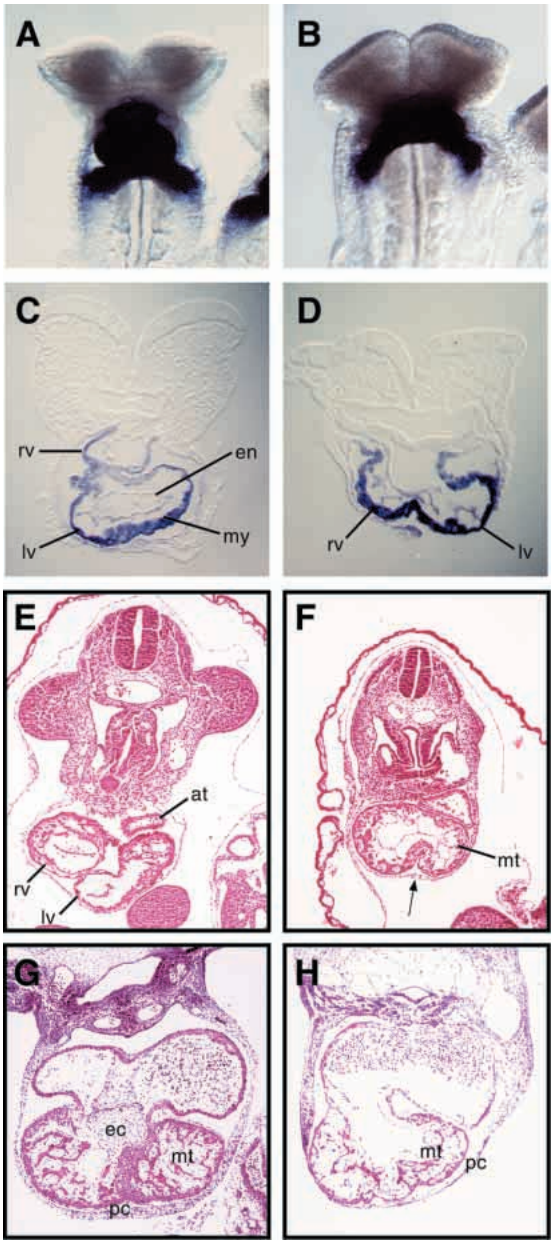

Fig. 8. Heart morphogenesis is affected by the loss of *Bmp5* and *Bmp7*. (A-D) 8.5 dpc, (E,F) 9.5 dpc, and (G,H) 10.5 dpc embryos. (A) Normal *MLC-2A* expression in a 10 somite embryo. (B) *MLC-2A* expression in a 10 somite *Bmp5;Bmp7* double mutant embryo. (C) Transverse section of the embryo in A showing development of the ventricles. (D) Comparable section to B showing a delay in separation of the ventricles. (E) Heart histology at 9.5 dpc in control embryo. (F) Double mutant littermate shows a lack of chamber septation and a reduction in myocardial trabeculation (arrow). (G) Endocardial cushions are well-formed by 10.5 dpc in control embryos. (H) No cushions are observed in double mutants at 10.5 dpc, and the heart has begun to degenerate. en, endocardium; my, myocardium; rv, right ventricle; lv, left ventricle; at, atrium; mt, myocardial trabeculation; ec, endocardial cushions; pc, pericardium.

Involvement of *Bmp5* and *Bmp7* in somitogenesis

Abnormalities in somitogenesis in double mutants were first apparent by 9.5 dpc; 80% (18/22) of the double mutants examined contained 'ectopic' somites situated on either side of the neural tube in the vicinity of the forelimb bud. Interestingly, these somites were individually much smaller than adjacent normal somites but occupied a similar area when considered as pairs (dorsal somite plus ectopic mediolateral somite). Their small size suggests that the ectopic somites form by fragmenting away from a normally sized somite. By 10.5 dpc, the somites in the region of the forelimb bud often appear more fragmented and disorganized, and *Fgf-8* transcripts are undetectable in the lateral myotome (Fig. 5D). The absence of *Fgf-8* expression in the rostral and caudal margins of each somite demonstrates that later somite development is also aberrant or delayed in *Bmp5*;*Bmp7* mutant embryos.

Pax3 is expressed in the presomitic mesoderm and the dorsal halves of the epithelial somites (Fig. 9A; Goulding et al., 1991). Upon de-epithelialization of the somite, *Pax3* expression becomes restricted to the ventrolateral domain of the dermomyotome (Fig. 9B,C). *Pax3* transcripts are also localized along the length of the dorsal neural tube. Comparison of 8.5 dpc (12-15 somite) embryos failed to reveal any abnormalities in the localization of *Pax3* in *Bmp5;Bmp7* double mutants (Fig. 9A). By 9.5 dpc, however, the domain of *Pax3* expression in the somites adjacent to the forelimb bud has split into two distinct territories (Fig. 9B). Somites 12 through 18 are most commonly affected in the double mutants, whereas somites rostral and caudal to this region display normal localization of *Pax3*. In normal 9.5 dpc embryos the somites have already differentiated into sclerotome, myotome and dermomyotome (Fig. 9G), whereas most of the somites in the *Bmp5/Bmp7* double mutants remain epithelialized (Fig. 9D). Rarely, double mutants were found to have initiated somite de-epithelialization, but unlike controls, the sclerotomal component of each somite was morphologically distinct from its surroundings (Fig. 9E,F). Despite this apparent delay in somitogenesis, *Pax3* transcripts are correctly localized to the dorsal halves of these somites. In addition, we note that the 'split' somites observed in the double mutants appear as two distinct epithelialized structures (Fig. 9H) with *Pax3* transcripts expressed along their dorsomedial edges (Fig. 9D). The observation that *Pax3* is expressed normally at 8.5 dpc in

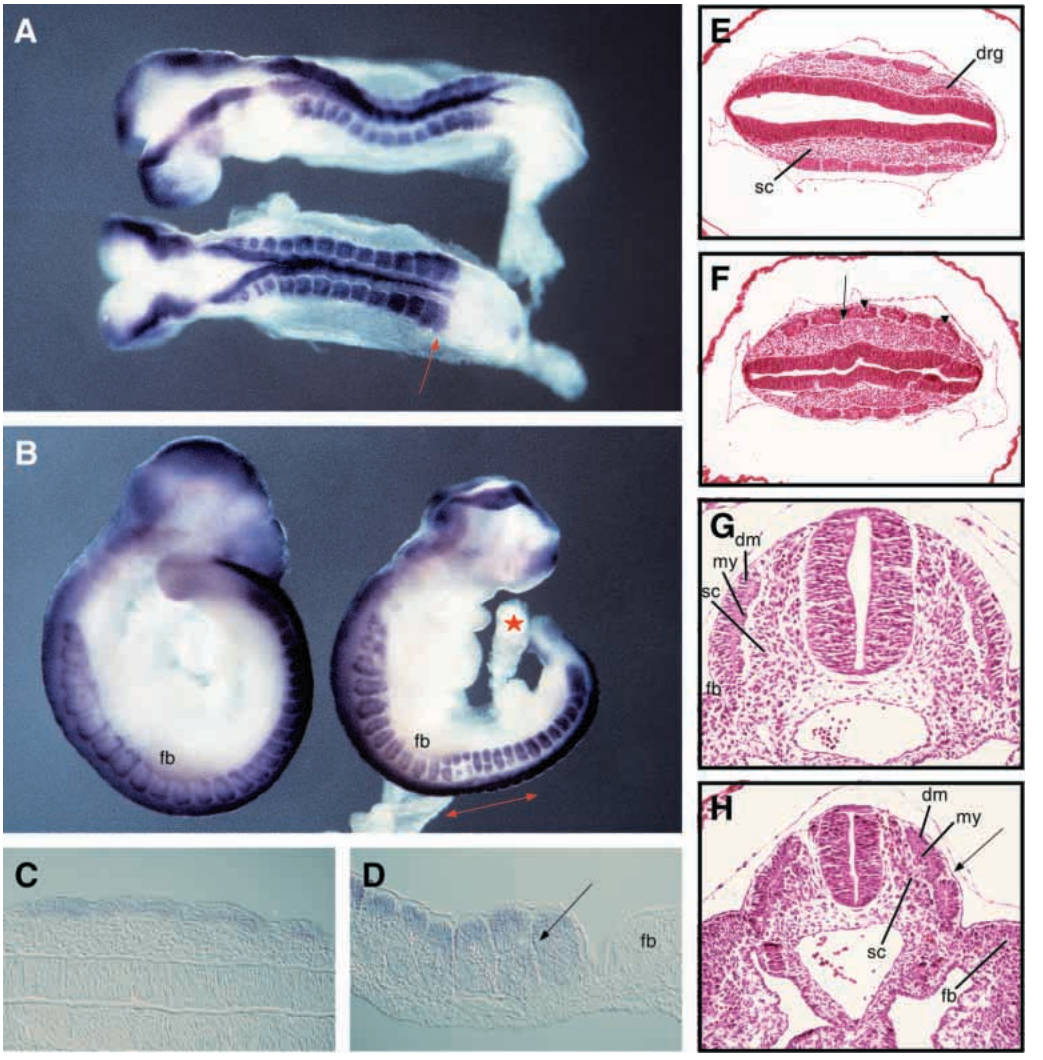

Fig. 9. The development of a subset of somites is aberrant in *Bmp5;Bmp7* mutant embryos. (A) *Pax-3* is expressed normally in the dermomyotome and dorsal neural tube of 12 somite mutant (lower) and control embryos. (B) *Pax3* expression reveals abnormalities in somite development in *Bmp5;Bmp7* embryos (right) at 9.5 dpc. The 6-8 somites overlying and caudal to the forelimb bud often show discontinuity in *Pax-3* expression midway along the mediolateral axis of the somite (double-headed arrow). This defect occurs bilaterally and rarely affects other somites. Also note the unfused allantois of the mutant (star). (C,D) Cross sections through the embryos in B. (C) *Pax-3* transcripts are restricted to the dermomyotome in control embryos. (D) *Pax-3* expression is correctly localized to the dermomyotome of mutant somites, although in this embryo the somites remain epithelialized and are 'split' (arrow). (E,F) Histological analysis of rostral somites at 9.5 dpc in (E) control and (F) mutant embryos. Mutants exhibit fissures in the sclerotome (arrows), reduced dorsal root ganglia, a kinked neural tube, and a separation of the dermomyotome and myotome (arrowheads). (G,H) Transverse sections through somites at the level of the forelimb bud at 9.5 dpc. (G) Control embryo. (H) The dermomyotomal and myotomal components of the affected somites in the double mutants form a continuous layer at the fissure site. fb, forelimb bud; sc, sclerotome; drg, dorsal root ganglion; dm, dermomyotome; my, myotome.

somites 12-15 in the double mutants implies that the supernumerary somites did not arise *de novo* during somitogenesis.

mTwist, initially expressed throughout the epithelial somites at 8.0 dpc, becomes restricted to the ventromedial half of the somite fated to give rise to the sclerotome by 8.5 dpc. At 9.5 dpc, *mTwist* continues to be expressed in the sclerotome and is again observed in the dermomyotome (Füchtbauer, 1995). Analysis of this marker further confirmed the defects observed in the *Pax3* whole mounts (Fig. 6B-D) and demonstrated that the split somites contained normally patterned sclerotome. We conclude from these results that *Bmp5* and *Bmp7* may directly impinge upon the developing somites, or alternatively, these signals may be required in the lateral plate, which in turn influences the development of the somites.

DISCUSSION

The widespread expression of members of the 60A subgroup of BMPs throughout mammalian development, together with their potent activities in vitro, suggests that these molecules function as essential regulators of growth and morphogenesis during embryogenesis (reviewed by Hogan, 1996). However, mutations in these genes have for the most part failed to support this hypothesis. Previous analysis of *Bmp5;Bmp6* double mutants reveals a subtle synergism during bone development (Solloway et al., 1998), but these genes are expressed primarily in adjacent, non-overlapping cell populations. We have described the coexpression of *Bmp5* and *Bmp7* from gastrulation onwards. Analysis of *Bmp5;Bmp7* double mutants reveals that these factors compensate for each other at early stages of embryonic development and uncovers novel requirements for BMP signaling in the allantois, heart, somites, branchial arches and forebrain.

Overlapping expression domains of *Bmp5* and *Bmp7*

The ubiquitous expression patterns of several type I BMP receptors (Dewulf et al., 1995; Ikeda et al., 1996) plus their varying affinities for different BMP ligands (ten Dijke et al.,

1994) indicates that most tissues have the capacity to receive BMP signals. The lack of data concerning the secretion, diffusion, reception and degradation of these factors in vivo makes it important to take into account expression in adjacent as well as identical tissues. *Bmp5* and *Bmp7* are coexpressed at a number of different sites during mouse development including the allantois, heart, branchial arches, lateral plate, and cranial neurectoderm and mesoderm. All of these tissues have the capacity to generate homodimers of *Bmp5* and *Bmp7* as well as *Bmp5/Bmp7* heterodimers. The wide overlap of *Bmp5* and *Bmp7* expression patterns suggested several tissues which may potentially be affected in the double mutants, and in keeping with this, mutant phenotypes are observed in virtually all of these sites.

Growth/apoptosis versus specification

Our data supports a model in which the BMPs act primarily as regulators of cell growth and death rather than instructive cues for cell specification during development. For example, the coexpression of *Bmp5* and *Bmp7* in the dorsal cranial neurectoderm coincides with areas of increased cell death during neural tube closure (Schlüter, 1973), and *Bmp5;Bmp7* mutants display an abnormal reduction of TUNEL-positive cells in the dorsal cranial folds (Fig. 4F). Interestingly, caspase inhibitors have been shown to block apoptosis in this region and prevent neural tube closure in the chick (Weil et al., 1997). Thus, the reduction in programmed cell death in the double mutant neurectoderm potentially explains the delay in rostral neural tube closure. However, this defect might also be due to a reduction in the proliferation of the cranial neurectoderm.

Recent data suggests that BMPs are important regulators of forebrain (Furuta et al., 1997; Shimamura and Rubenstein, 1997) and hindbrain (Arkell and Beddington, 1997) development. Ectopic expression of Bmp7 adjacent to the hindbrain causes expansion of dorsally restricted genes and promotes cell growth in the neurectoderm (Arkell and Beddington, 1997). Our analysis demonstrates that general dorsal/ventral and rostral/caudal boundaries are preserved in the *Bmp5;Bmp7* double mutant embryos. However, gross examination of these embryos and analysis of *Wnt8b* expression reveals a disproportionate reduction in the size of the telencephalon. Additionally, expression of the neural crest marker *AP-2* is transiently lost from the rostral-most neurectoderm in double mutants at 8.5 dpc, in correspondence with the onset of *Bmp5* and *Bmp7* expression in this tissue. The absence of ectopic apoptotic cells in the rostral neurectoderm makes it likely that this defect is caused by a specific reduction in the growth rate of the rostral neuroepithelium and/or cranial mesenchyme.

The absence of *Bmp5* and *Bmp7* may affect several tissues which contribute to branchial arch growth. Expression studies in the chick have implicated Bmp4 and Bmp7 in the regulation of the growth of the branchial arch (Wall and Hogan, 1995). BMPs have also been implicated in the formation (Liem et al., 1995; Arkell and Beddington, 1997) and death (Graham et al., 1994) of neural crest cells, a major component of the arches. We have shown that *Bmp5* and *Bmp7* are expressed in the nascent cranial mesenchyme and dorsal neurectoderm at 8.5 dpc, and thus could be involved in the early specification/growth of neural crest and mesoderm fated to contribute to the arches. However, *AP-2* localization reveals normal generation of cranial neural crest. The reduction in *Twist*-positive cells, in contrast, indicates that cranial mesenchyme development is aberrant in the double mutants and may affect the branchial arches. *Bmp5* and *Bmp7* are also localized to the ectoderm of the developing branchial arches and could potentially regulate the recruitment of cells and growth of the arches from this site as well. This hypothesis is supported by the dramatic increase in apoptosis observed in the ectodermal cells at the base of the first branchial arch in *Bmp5;Bmp7* mutants. These BMPs may also simply be required as autocrine maintenance/survival factors within these cells, and in their absence, the ectoderm fails to proliferate and correctly pattern the arch. Tissue recombination experiments will help to resolve which tissues require Bmp5 and Bmp7 activity for proper development of the branchial arches.

BMPs are expressed in the epidermal ectoderm cells adjacent to the neural plate (Liem et al., 1995; Lyons et al., 1995; Arkell and Beddington, 1997; Dudley and Robertson, 1997; Furuta et al., 1997), and roof plate differentiation and the induction of neural crest appears to be mediated in part by the BMPs (Liem et al., 1995; Liem et al., 1997). In keeping with this proposal, *Bmp5;Bmp7* double mutants display a significant reduction in the numbers of *AP-2*-positive trunk ganglia. However, two points argue that this phenotype may arise secondarily from defects in tissues other than the neural tube. Although *Bmp7* is expressed along the length of the dorsal neural tube and within the adjacent ectoderm, the nearest domains of *Bmp5* expression (the somites and the lateral plate mesoderm) are likely too far from the neural tube to have an influence on the production of neural crest. Additionally, neural crest emigrate normally from cultured neural tube isolated from double mutants. Thus, within the limits of this assay, neural crest precursor cells are correctly specified in the absence of Bmp5 and Bmp7. However, this assay does not preclude the involvement of these factors in the subsequent growth and differentiation of these cells.

Neural crest cells follow two routes from the dorsal neural tube, migrating either dorsally between the surface ectoderm and dermomyotome, or ventrally through the rostral, but not caudal, sclerotome (Bronner-Fraser, 1986). Thus, the rostrocaudal polarization of the somites directly influences neural crest migration. Interestingly, *Bmp5* expression within the somites becomes localized to the rostral and caudal quadrants of the sclerotome (Fig. 2G), and *Bmp5;Bmp7* mutants lack polarized expression of *Fgf8* in the lateral myotome. This indicates that somite development may be sufficiently perturbed by the absence of Bmp5 and Bmp7 to prevent normal neural crest migration. This fails to explain, however, the severe reduction in *AP-2*-positive cells along the mutant trunk.

Numerous experiments point to a role for BMPs in regulating early somite pattern. BMP signals derived from the dorsal neural tube (Marcelle et al., 1997) as well as the lateral plate (Pourquié et al., 1996; Tonegawa et al., 1997) are believed to regulate the patterning of the dermomyotomal compartment of the somite. Additional localization, mutational, and loss and gain of function studies of Noggin, a BMP-specific antagonist (Zimmerman et al., 1996), demonstrate that the local inhibition of BMP signaling is important for normal somite patterning (Hirsinger et al., 1997; Capdevila and Johnson, 1998; McMahon et al., 1998; Reshef et al., 1998). Double mutant embryos display normal somite formation at 8.5 dpc, but by 9.5 dpc the dermomyotome often splits along the rostrocaudal axis in the middle of the somites adjacent to the forelimb bud. Intriguingly, when *noggin*-expressing cells are placed in the

prospective lateral mesoderm near the primitive streak, supernumerary somites formed in a mediolateral direction (reported in Tajbakhsh and Spörle, 1998). However, as was the case for the branchial arches, it is difficult to determine whether these defects reflect a primary requirement for BMP signaling in the somite or a more general defect in the development of the lateral plate mesoderm.

Possible mechanisms of interaction

Our study clearly reveals cooperative signaling in the majority of tissues where *Bmp5* and *Bmp7* are coexpressed. Several non-mutually exclusive explanations can account for this interaction. First, a reduction in the overall level of BMP signaling could lead to delayed growth and development of tissues expressing both *Bmp5* and *Bmp7*. The promiscuity of BMP ligand/receptor interactions lends support to this hypothesis. Transfected cells expressing ALK-3 can bind Bmp2, Bmp4 and Bmp7 with variable affinities (ten Dijke et al., 1994). In addition, a large body of evidence demonstrates that members of the TGF-β superfamily can elicit a spectrum of concentration-dependent responses (Ferguson and Anderson, 1992; Green et al., 1992; Gurdon et al., 1994), although similar results have not been reported for the vertebrate BMPs (Arkell and Beddington, 1997; Shimamura and Rubenstein, 1997). Thus, the combination of mutations in two BMPs expressed in the same cells may lower the level of BMP signaling below an important threshold. However, recent experiments in our laboratory indicate that this explanation is too simple. *Bmp6*, another member of the 60A subfamily, is 87% identical to *Bmp7* in the C terminus and is coexpressed with *Bmp7* throughout the developing allantois (Furuta et al., 1997). Despite this, *Bmp6;Bmp7* double mutant embryos show normal chorioallantoic fusion and placental development at 11.5 dpc (M. J. S., R. Kim and E. J. R., unpublished results). These data indicate that different BMPs can have distinct genetic interactions (and thus different activities) in tissues in which they are coexpressed.

The combinatorial effect of mutations in *Bmp5* and *Bmp7* may also be due to a physical interaction between the two ligands. Ligands in the TGF-β superfamily are active as dimers, and the subunit composition of these molecules can dramatically affect signaling activity. A striking example of naturally occurring heterodimers comes from studies of the inhibin/activin subgroup of the TGF-β superfamily. Heterodimers of inhibin α and β chains (inhibins αβ) and homodimers of inhibin β chains (activins ββ) have opposite biological effects on many systems (for review see Vale et al., 1988). Although BMP heterodimers have yet to be identified in vivo, functional heterodimers made in vitro display significantly more activity than purified homodimers in bone and mesoderm induction assays (Aono et al., 1995; Suzuki et al., 1997). Recent experiments in *Xenopus* also attribute unique activities to BMP heterodimers: heterodimeric BMP-4/7 protein directly induces mesoderm in isolated animal caps, whereas homodimeric BMPs or mixtures of homodimers fail to induce any mesodermal markers (Nishimatsu and Thomsen, 1998). These functional differences potentially reflect resistance of the heterodimers to degradation, higher affinity for a receptor complex, and/or altered affinities for different receptors. Unfortunately, due to the promiscuity of ligand/ligand and ligand/receptor interactions, overexpression or misexpression assays are of limited utility in determining the biological relevance of heterodimers. It will be interesting to learn more about Bmp5/Bmp7 heterodimer signaling under physiological conditions in vivo.

Recent experiments in *Drosophila* also provide strong evidence for the in vivo interaction of different members of the TGF-β superfamily. A genetic screen for modifiers of a hypomorphic allele of *thick veins* (*tkv*), a type I receptor for *dpp*, uncovered mutations in the *60A* gene (Chen et al., 1998), and further experiments demonstrated synergistic interactions between *dpp*- and *60A*-specific pathways (Haerry et al., 1998; Khalsa et al., 1998). Similarly, *screw* (*scw*), a ubiquitously expressed TGF-β family member, was originally proposed to upregulate *dpp* activity by forming Scw/Dpp heterodimers which function in the dorsal/ventral patterning of the embryonic ectoderm (Arora et al., 1994; Raftery et al., 1995). However, misexpression of *scw* in cells which do not express *dpp* is sufficient to rescue a *scw* mutant, suggesting that Dpp/Scw heterodimers are not essential for generation of the early axis (Neul et al., 1998; Nguyen et al., 1998). It is important to note that these observations do not preclude heterodimer formation between Scw and another as-yet-unidentified TGF-β ligand. Regardless of the mechanism used, these experiments unambiguously demonstrate that one TGF-β ligand can modify signaling from a distinct ligand. We have shown that *Bmp7* is generally expressed more broadly throughout the embryo than *Bmp5* (Figs 1 and 2). Thus, by analogy to *scw* and *dpp*, the localization of *Bmp5* may serve to potentiate or refine cellular responses within a subdomain of *Bmp7*. Alternatively, the broad distribution of *Bmp7* may function to increase the strength of signaling from a limited amount of *Bmp5* that diffuses from its site of synthesis. The late-onset phenotypes in single *Bmp5* or *Bmp7* null animals indicate, however, that the direct interaction of *Bmp5*- and *Bmp7*-dependent signals is not required for early development. Instead, it is likely that these signals also impinge on pathways downstream from other distinct BMP ligands, and it is the combined loss of these signals which cause the phenotypes observed in the double mutants.

Bmp5 and *Bmp7* may also synergize via the interaction of downstream effector molecules. Experiments using chimeric erythropoietin/TGF-β receptors show that homodimerization of type I receptors and hetero-oligomerization with type II receptors are required for efficient signal transduction (Luo and Lodish, 1996). This result is supported by the isolation of a heterotetramer consisting of two TβR-I and two TβR-II molecules (Yamashita et al., 1994). It is presently not known whether two different type I or type II receptors can interact with the same complex, but if this were true, it would provide a simple mechanism to simultaneously sense different levels of ligands to elicit distinct responses. Similarly, the three-dimensional structure of the MH2 domain of Smad4 indicates that SMADs form homotrimers which form hexamers with a different SMAD homotrimer in response to receptor activation (Hata et al., 1997; Shi et al., 1997), and the same arguments can be used for multiple BMP inputs leading to the formation of heterotrimers with unique activities. Different SMADs have also been shown to synergize in response to receptor stimulation (Zhang et al., 1996b). Similarly, Smad4 can interact with Smad2 and Smad3, while Smad2 can also interact with Smad3 in a TGF-β-dependent manner (Nakao et al., 1997). Thus Bmp5 and Bmp7 may activate different complements of SMADs which subsequently interact. Additionally, different BMP ligands could stimulate different receptors which in tandem lead to

distinct phosphorylation patterns of a target SMAD. The finding that ERK kinase can phosphorylate Smad1 and oppose TGF-β-stimulated phosphorylation (Kretzschmar et al., 1997) lends support to this model.

The generation of mice bearing mutations in different pairs of related genes has proven to be a powerful and effective means of ascribing shared and unique functions to these genes and placing them within pathways. Our studies reveal novel functions for *Bmp5* and *Bmp7* during early mouse development. The sites of genetic interaction directly correlate to regions of overlapping expression of *Bmp5* and *Bmp7*, indicating that these factors act locally during development. Our analysis is the first in vivo confirmation that BMP molecules can functionally compensate for each other during development. Further analysis of different mutant combinations, as well as more subtle misexpression or site-specific ablation studies, should greatly increase our appreciation for the multitude of tissues affected by BMP signaling. In addition, having demonstrated a requirement for *Bmp5*- and *Bmp7*-dependent signaling in the development of several distinct tissues, we can now begin to dissect the interactions between the signaling pathways downstream of each ligand.

We are grateful to David Kingsley for providing *Bmp5* probes, Scott Lee and Andrew McMahon for sharing their unpublished probe for *Wnt8b*, and Richard Harvey for providing us with various heart markers. We thank Patti Lewko and Joe Rocca for providing expert animal care, Debbie Pelusi and Rebecca Kim for technical assistance, and Liz Bikoff and Daniel Constam for thoughtful comments on the manuscript. M. J. S. was funded in part by a National Research Service Award training grant from the National Institutes of Health (GM07620). This work was also supported by a grant from the NIH (HD25208) to E. J. R.

REFERENCES

Aono, A., Hazama, M., Notoya, K., Taketomi, S., Yamasaki, H., Tsukuda, R., Sasaki, S. and Fujisawa, Y. (1995). Potent ectopic bone-inducing activity of Bone Morphogenetic Protein-4/7 heterodimer. *Bichem. Biophys. Res. Comm.* **210,** 670-677.

Arkell, R. and Beddington, R. S. P. (1997). BMP-7 influences pattern and growth of the developing hindbrain of mouse embryos. *Development* **124,** 1-12.

Arora, K., Levine, M. S. and O'Connor, M. B. (1994). The screw gene encodes a ubiquitously expressed member of the TGF-beta family required for specification of dorsal cell fates in the Drosophila embryo. *Genes Dev.* **8,** 2588-2601.

Bellusci, S., Henderson, R., Winnier, G., Oikawa, T. and Hogan, B. L. (1996). Evidence from normal expression and targeted misexpression that bone morphogenetic protein (Bmp-4) plays a role in mouse embryonic lung morphogenesis. *Development* **122,** 1693-1702.

Bronner-Fraser, M. (1986). Analysis of the early stages of trunk neural crest migration in avian embryos using monoclonal antibody HNK-1. *Dev. Biol.* **115,** 44-55.

Capdevila, J. and Johnson, R. L. (1998). Endogenous and ectopic expression of noggin suggests a conserved mechanism for regulation of BMP function during limb and somite patterning. *Dev. Biol.* **197,** 205-217.

Chen, Y., Riese, M. J., Killinger, M. A and Hoffmann, F. M. (1998). A genetic screen for modifiers of Drosophila decapentaplegic signaling identifies mutations in punt, Mothers against dpp and the BMP-7 homologue, 60A. *Development* **125,** 1759-1768.

Chen, Z. F. and Behringer, R. R. (1995). twist is required in head mesenchyme for cranial neural tube morphogenesis. *Genes Dev.* **9,** 686-699.

Conlon, R. A., Reaume, A. G. and Rossant, J. (1995). Notch1 is required for the coordinate segmentation of the somites. *Development* **121,** 1533-1545.

Dewulf, N., Verschueren, K., Lonnoy, O., Moren, A., Grimsby, S., Vande Spiegle, K., Miyazono, K., Huylebroeck, D. and ten Dijke, P. (1995). Distinct spatial and temporal patterns of two type I receptors for bone morphogenetic proteins during mouse embryogenesis. *Endo.* **136,** 2652-2653.

Dudley, A. T., Lyons, K. M. and Robertson, E. J. (1995). A requirement for bone morphogenetic protein-7 during development of the mouse mammalian kidney and eye. *Genes Dev.* **9,** 2795-2807.

Dudley, A. T. and Robertson, E. J. (1997). Overlapping expression domains of bone morphogenetic protein family members potentially account for limited tissue defects in *BMP7* deficient embryos. *Dev. Dyn.* **208,** 349-362.

Echelard, Y., Epstein, D. J., St-Jacques, B., Shen, L., Mohler, J., McMahon, J. A. and McMahon, A. P. (1993). Sonic Hedgehog, a member of a family of putative signaling molecules, is implicated in the regulation of CNS polarity. *Cell* **75,** 1417-1430.

Ferguson, E. L. and Anderson, K. V. (1992). Decapentaplegic acts as a morphogen to organize dorsal-ventral pattern in the Drosophila embryo. *Cell* **71,** 451-461.

Fishman, M. C. and Chien, K. R. (1997). Fashioning the vertebrate heart: earliest embryonic decisions. *Development* **124,** 2099-2117.

Füchtbauer, E. M. (1995). Expression of M-twist during postimplantation development of the mouse. *Dev. Dyn.* **204,** 316-322.

Furuta, Y., Piston, D. W. and Hogan, B. L. (1997). Bone Morphogenetic Proteins (BMP's) as regulators of dorsal forebrain development. *Development* **124,** 2203-2212.

Gañan, Y., Macias, D., Duterque-Coquillaud, M., Ros, M. A. and Hurle, J. M. (1996). Role of TGF beta s and BMPs as signals controlling the position of the digits and the areas of interdigital cell death in the developing chick limb autopod. *Development* **122,** 2349-2357.

Geelen, J. A. and Langman, J. (1977). Closure of the neural tube in the cephalic region of the mouse embryo. *Anat. Rec.* **189,** 625-640.

Goulding, M. D., Chalepakis, G., Detsch, U., Erselius, J. R. and Gruss, P. (1991). Pax-3, a novel murine DNA binding protein expressed during early neurogenesis. *EMBO J.* **10,** 1135-1147.

Graham, A., Francis-West, P., Brickell, P. and Lumsden, A. (1994). The signaling molecule BMP-4 mediates apoptosis in the rhombencephalic neural crest. *Nature* **372,** 684-686.

Green, E. L. and Green, M. C. (1942). The Development of Three Manifestations of the Short Ear Gene in the Mouse. *J. Morphol.* **70,** 1-19.

Green, M. C. (1951). Further morphological effects of the short ear gene in the house mouse. *J. Morphol.* **88,** 1-21.

Green, J. B., New, H. V. and Smith, J. C. (1992). Responses of embryonic Xenopus cells to activin and FGF are separated by multiple dose thresholds and correspond to distinct axes of the mesoderm. *Cell* **71,** 731-739.

Gurdon, J. B., Harger, P., Mitchell, A. and Lemaire, P. (1994). Activin signalling and response to a morphogen gradient. *Nature* **371,** 487-492.

Gurtner, G. C., Davis, V., Li, H., McCoy, M. J., Sharpe, A. and Cybulsky, M. I. (1995). Targeted disruption of the murine VCAM1 gene: essential role of VCAM-1 in chorioallantoic fusion and placentation. *Genes Dev.* **9,** 1-14.

Haerry, T. E., Khalsa, O., O'Connor, M. B. and Wharton, K. A. (1998). Synergistic signaling by two BMP ligands through the SAX and TKV receptors controls wing growth and patterning in *Drosophila. Development* **125,** 3977-3987.

Hata, A., Lo, R. S., Wotton, D., Lagna, G. and Massagué, J. (1997). Mutations increasing autoinhibition inactivate tumour suppressors Smad2 and Smad4. *Nature* **388,** 82-87.

Heikinheimo, M., Lawshé, A., Shackleford, G. M., Wilson, D. B. and MacArthur, C. A. (1994). Fgf-8 expression in the post-gastrulation mouse suggests roles in the development of the face, limbs, and central nervous system. *Mech. Dev.* **48,** 129-138.

Hirsinger, E., Duprez, D., Jouve, C., Malapert, P., Cooke, J. and Pourquié, O. (1997). Noggin acts downstream of Wnt and Sonic Hedgehog to antagonize BMP4 in avian somite patterning. *Development* **124,** 4605-4614.

Hogan, B. L. M. (1996). Bone morphogenetic proteins: multifunctional regulators of vertebrate development. *Genes Dev.* **10,** 1580-1594.

Ikeda, T., Takahashi, H., Suzuki, A., Ueno, N., Yokose, S., Yamaguchi, A. and Yoshiki, S. (1996). Cloning of rat type I receptor cDNA for Bone Morphogenetic Protein-2 and Bone Morphogenetic Protein-4, and the localization compared with that of the ligands. *Dev. Dyn.* **206,** 318-329.

Jeffs, P. and Osmond, M. (1992). A segmented pattern of cell death during development of the chick embryo. *Anat. Embryol. (Berl)* **185,** 589-598.

Khalsa, O., Yoon, J. W., Torres-Schumann, S. and Wharton, K. A. (1998). TGF-beta/BMP superfamily members, Gbb-60A and Dpp, cooperate to provide pattern information and establish cell identity in the Drosophila wing. *Development* **125,** 2723-2734.

King, J. A., Marker, P. C., Seung, K. J. and Kingsley, D. M. (1994). BMP5

and the molecular, skeletal, and soft-tissue alterations in *short ear* mice. *Dev. Biol.* **166,** 112-122.

Kingsley, D. M., Bland, A. E., Grubber, J. M., Marker, P. C., Russell, L. B., Copeland, N. G. and Jenkins, N. (1992). The mouse *short ear* skeletal morphogenesis locus is associated with defects in a bone morphogenetic member of the TGFβ Superfamily. *Cell* **71,** 399-410.

Kretzschmar, M., Doody, J. and Massague, J. (1997). Opposing BMP and EGF signalling pathways converge on the TGF-beta family mediator Smad1. *Nature* **389,** 618-622.

Kretzschmar, M. and Massagué, J. (1998). SMADs: mediators and regulators of TGF-beta signaling. *Curr. Opin. Genet. Dev.* **8,** 103-111.

Kubalak, S. W., Miller-Hance, W. C., O'Brien, T. X., Dyson, E. and Chien, K. R. (1994). Chamber specification of atrial myosin light chain-2 expression precedes septation during murine cardiogenesis. *J. Biol. Chem.* **269,** 16961-70.

Kwee, L., Baldwin, H. S., Shen, H. M., Stewart, C. L., Buck, C., Buck, C. A. and Labow, M. A. (1995). Defective development of the embryonic and extraembryonic circulatory systems in vascular cell adhesion molecule (VCAM-1) deficient mice. *Development* **121,** 489-503.

Liem, K. F., Tremml, G., Roelink, H. and Jessell, T. M. (1995). Dorsal differentiation of neural plate cells induced by BMP-mediated signals from epidermal ectoderm. *Cell* **82,** 969-979.

Liem, K. F. J., Tremml, G. and Jessell, T. M. (1997). A role for the roof plate and its resident TGFbeta-related proteins in neuronal patterning in the dorsal spinal cord. *Cell* **91,** 127-138.

Luo, G., Hofmann, C., Bronckers, A. L. J. J., Sohocki, M., Bradley, A. and Karsenty, G. (1995). BMP-7 is an inducer of nephrogenesis, and is also required for eye development and skeletal patterning. *Genes Dev.* **9,** 2808-2820.

Luo, K. and Lodish, H. F. (1996). Signaling by chimeric erythropoietin-TGF-beta receptors: homodimerization of the cytoplasmic domain of the type I TGF-beta receptor and heterodimerization with the type II receptor are both required for intracellular signal transduction. *EMBO J.* **15,** 4485-4496.

Lyons, K. M., Hogan, B. L. M. and Robertson, E. J. (1995). Colocalization of BMP 7 and BMP 2 RNAs suggests that these factors cooperatively mediate tissue interactions during murine development. *Mech. Dev.* **50,** 71-83.

Marcelle, C., Stark, M. R. and Bronner-Fraser, M. (1997). Coordinate actions of BMPs, Wnts, Shh and noggin mediate patterning of the dorsal somite. *Development* **124,** 3955-3963.

Massagué, J. (1998). TGF-beta signal transduction. *Annu. Rev. Biochem.* **67,** 753-791.

McMahon, J. A., Takada, S., Zimmerman, L. B., Fan, C. M., Harland, R. M. and McMahon, A. P. (1998). Noggin-mediated antagonism of BMP signaling is required for growth and patterning of the neural tube and somite. *Genes Dev.* **12,** 1438-1452.

Mishina, Y., Suzuki, A., Ueno, N. and Behringer, R. R. (1995). Bmpr encodes a type I Bone morhogenetic protein receptor that is essential for gastrulation during mouse embryogenesis. *Genes Dev.* **9,** 3027-3037.

Mitchell, P. J., Timmons, P. M., Hébert, J. M., Rigby, P. W. and Tjian, R. (1991). Transcription factor AP-2 is expressed in neural crest cell lineages during mouse embryogenesis. *Genes Dev.* **5,** 105-119.

Nakao, A., Imamura, T., Souchelnytskyi, S., Kawabata, M., Ishisaki, A., Oeda, E., Tamaki, K., Hanai, J., Heldin, C. H., Miyazono, K. and ten Dijke, P. (1997). TGF-beta receptor-mediated signalling through Smad2, Smad3 and Smad4. *EMBO J.* **16,** 5353-5362.

Neul, J. L. and Ferguson, E. L. (1998). Spatially restricted activation of the SAX receptor by SCW modulates DPP/TKV signaling in Drosophila dorsal-ventral patterning. *Cell* **95,** 483-494.

Nguyen, M., Park, S., Marques, G. and Arora, K. (1998). Interpretation of a BMP activity gradient in Drosophila embryos depends on synergistic signaling by two type I receptors, SAX and TKV. *Cell* **95,** 495-506.

Nishimatsu, S. and Thomsen, G. H. (1998). Ventral mesoderm induction and patterning by bone morphogenetic protein heterodimers in Xenopus embryos. *Mech. Dev.* **74,** 75-88.

Parr, B. A., Shea, M. J., Vassileva, G. and McMahon, A. P. (1993). Mouse Wnt genes exhibit discrete domains of expression in the early embryonic CNS and limb buds. *Development* **119,** 247-261.

Pourquié, O., Fan, C. M., Coltey, M., Hirsinger, E., Watanabe, Y., Bréant, C., Francis-West, P., Brickell, P., Tessier-Lavigne, M. and Le Douarin, N. M. (1996). Lateral and axial signals involved in avian somite patterning: a role for BMP4. *Cell* **84,** 461-471.

Raftery, L. A., Twombly, V., Wharton, K. and Gelbart, W. M. (1995). Genetic screens to identify elements of the decapentaplegic signaling pathway in Drosophila. *Genetics* **139,** 241-254.

Reshef, R., Maroto, M. and Lassar, A. B. (1998). Regulation of dorsal somitic cell fates: BMPs and Noggin control the timing and pattern of myogenic regulator expression. *Genes Dev.* **12,** 290-303.

Schlüter, G. (1973). Ultrastructural observations on cell necrosis during formation of the neural tube in mouse embryos. *Z. Anat. Entwicklungsgesch.* **141,** 251-264.

Shah, N. M., Groves, A. L. and Anderson, D. J. (1996). Alternative neural crest cell fates are instructively promoted by TGFβ superfamily members. *Cell* **85,** 331-344.

Shi, Y., Hata, A., Lo, R. S., Massagué, J. and Pavletich, N. P. (1997). A structural basis for mutational inactivation of the tumour suppressor Smad4. *Nature* **388,** 87-93.

Shimamura, K. and Rubenstein, J. L. (1997). Inductive interactions direct early regionalization of the mouse forebrain. *Development* **124,** 2709-2718.

Solloway, M. J., Dudley, A. T., Bikoff, E. K., Lyons, K. M., Hogan, B. L. and Robertson, E. J. (1998). Mice lacking Bmp6 function. *Dev. Genet.* **22,** 321-339.

Song, Q., Mehler, M. F. and Kessler, J. A. (1998). Bone morphogenetic proteins induce apoptosis and growth factor dependence of cultured sympathoadrenal progenitor cells. *Dev. Biol.* **196,** 119-127.

Stemple, D. L. and Anderson, D. J. (1992). Isolation of a stem cell for neurons and glia from the mammalian neural crest. *Cell* **71,** 973-985.

Suzuki, A., Kaneko, E., Maeda, J. and Ueno, N. (1997). Mesoderm induction by BMP-4 and -7 heterodimers. *Biochem. Biophys. Res. Commun.* **232,** 153-156.

Tajbakhsh, S. and Spörle, R. (1998). Somite development: constructing the vertebrate body. *Cell* **92,** 9-16.

ten Dijke, P., Yamashita, H., Sampath, T. K., Reddi, A. H., Estevez, M., Riddle, D. L., Ichijo, H., Heldin, C. H. and Miyazono, K. (1994). Identification of type I receptors for osteogenic protein-1 and bone morphogenetic protein-4. *J. Biol. Chem.* **269,** 16985-16988.

Tonegawa, A., Funayama, N., Ueno, N. and Takahashi, Y. (1997). Mesodermal subdivision along the mediolateral axis in chicken controlled by different concentrations of BMP-4. *Development* **124,** 1975-1984.

Vale, W., Rivier, C., Hsueh, A., Campen, C., Meunier, H., Bicsak, T., Vaughan, J., Corrigan, A., Bardin, W. and Sawchenko, P., et. al. (1988). Chemical and biological characterization of the inhibin family of protein hormones. *Recent Prog. Horm. Res.* **44,** 1-34.

Waldrip, W. R., Bikoff, E. K., Hoodless, P. A., Wrana, J. L. and Robertson, E. J. (1998). Smad2 signaling in extraembryonic tissues determines anterior-posterior polarity of the early mouse embryo. *Cell* **92,** 797-808.

Wall, N. A. and Hogan B. L. M. (1995). Expression of bone morphogenetic protein-4 (BMP-4), bone morphogenetic protein-7 (BMP-7), fibroblast growth factor-8 (FGF-8) and sonic hedgehog (SHH) during branchial arch development in the chick. *Mech. Dev.* **53,** 383-392.

Weil, M., Jacobson, M. D. and Raff, M. C. (1997). Is programmed cell death required for neural tube closure? *Curr. Biol.* **7,** 281-284.

Wilkinson, D. G. (1992). *Whole-mount in Situ Hybridization of Vertebrate Embryos.* IRL Press, Oxford.

Winnier, G., Blessing, M., Labosky, P. A. and Hogan, B. L. M. (1995). Bone morphogenetic protein-4 is required for mesoderm formation and patterning in the mouse. *Genes Dev.* **9,** 2105-2116.

Yamashita, H., ten Dijke, P., Franzen, P., Miyazono, K. and Heldin, C. H. (1994). Formation of hetero-oligomeric complexes of type I and type II receptors for transforming growth factor-beta. *J. Biol. Chem.* **269,** 20172-20178.

Yang, J. T., Rayburn, H. and Hynes, R. O. (1995). Cell adhesion events mediated by alpha 4 integrins are essential in placental and cardiac development. *Development* **121,** 549-560.

Zhang, H. and Bradley, A. (1996). Mice deficient for BMP2 are nonviable and have defects in amnion/chorion and cardiac development. *Development* **122,** 2977-2986.

Zhang, J., Hagopian-Donaldson, S., Serbedzija, G., Elsemore, J., Plehn-Dujowich, D., McMahon, A. P., Flavell, R. A. and Williams, T. (1996a). Neural tube, skeletal and body wall defects in mice lacking transcription factor AP-2. *Nature* **381,** 238-241.

Zhang, Y., Feng, X., We, R. and Derynck, R. (1996b). Receptor-associated Mad homologues synergize as effectors of the TGF-beta response. *Nature* **383,** 168-172.

Zimmerman, L. B., De Jesus-Escobar, J. M. and Harland, R. M. (1996). The Spemann organizer signal noggin binds and inactivates bone morphogenetic protein 4. *Cell* **86,** 599-606.